THE LIFT FORCE ON A CIRCULAR CYLINDER OSCILLATING SINUSOIDALLY IN WATER

A Thesis

Presented to

the Faculty of the Department of Mechanical Engineering

University of Houston

In Partial Fulfillment

of the Requirements for the Degree

Master of Science in Mechanical Engineering

---

by

Jim Westerheid

July 1977

ACKNOWLEDGEMENTS

The support of many was necessary to complete this work. The shop staff of the Department of Mechanical Engineering, Messrs. Baklik, Mate, and Gates were very cooperative in making the test rig and set up of the electronics. Professor C. Dalton was very helpful and supportive during the work as were Professors J. M. Nash and G. H. Koopmann.

The support of my superiors at work was essential for the effort to be possible at all and the morale support of my wife, Ellen, were very welcomed.

THE LIFT FORCE ON A CIRCULAR CYLINDER OSCILLATING SINUSOIDALLY IN WATER

An Abstract of a Thesis

Presented to

The Faculty of the Department of Mechanical Engineering

University of Houston

In Partial Fulfillment

of the Requirements for the Degree

Master of Science in Mechanical Engineering

---

by

Jim Westerheid

July 1977

ABSTRACT

This research investigates transverse or lift forces acting on a circular cylinder in an oscillating flow. The cylinder itself is oscillated with simple harmonic motion in water which is otherwise at rest. The response of the cylinder to forces imposed by vortex formation and shedding were studied in the time domain. From the data obtained, predictions of forcing frequency due to the shedding and maximum peak force were obtained. Data was correlated to a nondimensional grouping consisting of Keulegan-Carpenter Number and Reynolds Number.

The test cylinder was a smooth 2 inch nominal diameter cylinder 13.37 inches long. Oscillation periods of 0.87 to 5.00 seconds were encountered and Keulegan-Carpenter Numbers of 6.28, 9.42, 12.57, 15.71, and 18.8 where obtained. Values of Reynolds Number ranged from 8.38×10^3 to 6.37×10^4.

Maximum peak values of lift coefficients ranged from 1.39 for Keulegan-Carpenter Number of 18.8 to 0.14 at Keulegan-Carpenter Number of 6.28.

The results were in general agreement with those obtained by other methods.

TABLE OF CONTENTS

LIST OF FIGURES

LIST OF TABLES

CHAPTER 1

INTRODUCTION

The knowledge of what happens to structural members in an oscillating flow field is of great importance. More and more structures such as offshore platforms are being built with longer members. In general, this increased length leads to lower stiffness and lower natural frequency of the member. When these variables are in a lower range, shedding of vortices and transverse vibrations caused by these vortices becomes more and more important. This is because the driving frequency, due to alternately shed vortices, gets closer to the natural frequency of the members.

The economics of not overdesigning are obvious. Before more economical designs of structures can be produced, more knowledge is needed concerning the forces.

The in-line drag and inertia forces have been extensively studied. Hunt [2] used an oscillating cylinder in a water tank at rest. He measured the in-line forces and obtained plots relative to velocity. He then correlated the velocity dependent force coefficient to R and $d/\sqrt{\nu\tau}$ where R is Reynolds number ($R = Ud/\nu$), U is free stream velocity, d is diameter, and ν is kinematic viscosity. The other parameter contains d and ν plus the period of oscillation τ.

Hunt found that the inertia force component of in-line force predominated over the drag force at lower values of amplitude to diameter ratio. At higher velocities and stroke, the drag force began to be a substantial portion of the result. He also found that the maximum force came before maximum velocity. This is reasonable because of the dominance of the acceleration-dependent inertia force and the 90° phase difference between acceleration and velocity. By correlating the data to a nondimensional relationship, Hunt found that the force coefficient was asymptotic to a steady flow value of 1.2 at higher amplitude to diameter ratios. At lower amplitude to diameter ratios, the inertia force's predominance prevents this trend to a steady value of drag coefficient. The nondimensional groupings chosen by Hunt are

$$\frac{F/L}{\rho d\ U^2} = \Phi\left(\frac{Ud}{\nu},\ \frac{d}{\sqrt{\nu\tau}}\right) \tag{1}$$

where F is force, L is cylinder length, U is freestream velocity, ρ is density of the fluid, d is cylinder diameter, ν is kinematic viscosity and τ is the oscillation period. Sarpkaya [1] also measured in-line forces.

Sarpkaya states that asymmetric vortex shedding causes asymmetry in the in-line force and transverse force. This

asymmetric shedding is described and illustrated in Figure 1. When compared against the Keulegan-Carpenter number, K, there are defined ranges of this number that give predictable vortex shedding characteristics. K is a function of velocity, oscillation period, and cylinder diameter. Along with other governing parameters, it will be discussed in the next few pages and defined functionally.

As Figure 1 shows there is no separation at K of 2 or less. Between values of 2 and 4 for K, according to Issacson and Maull [4], separation occurs and vorticity develops. In the range of 2 to 4, a transition occurs in forming the vortex due to separation and backflow behind the cylinder. The slightest disturbance can trigger a vortex between K of 2 or 4 but separation is not predictable until K of 4 or greater. Between K values of 4 and 6, vortex formation remains symmetric and no shedding occurs. No lift occurs below values of $K = 6$. Between values of 6 and 15 for K, one vortex is shed each half cycle and asymmetry in forces is introduced. Asymmetry occurs because the vortex that is shed gives additional relative velocity to the fluid when the cylinder reverses direction. As the cylinder moves back through the disturbed region, the side of the shed vortex will develop the stronger vortex again

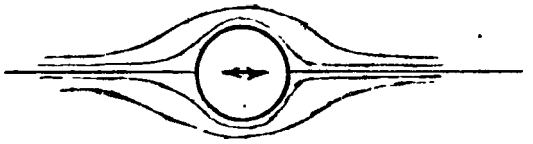

K<2 NO SEPARATION

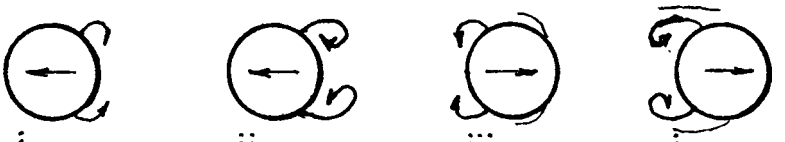

4>K<6 NO VORTEX DETACHMENT
NO LIFT

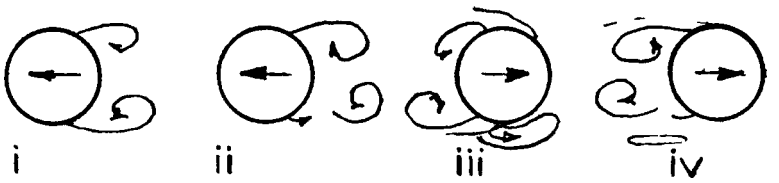

K=8 ONE VORTEX SHED
PER HALF CYCLE

ASYMMETRIC LIFT

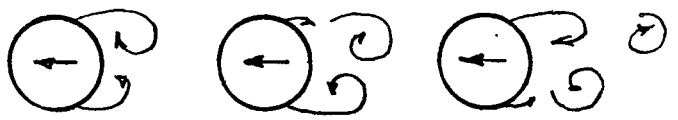

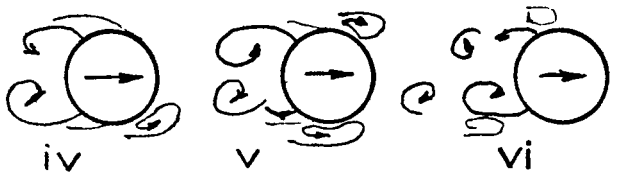

K=15 TWO VORTICES
PER HALF CYCLE

SYMMETRIC LIFT

VORTEX FORMATION FIGURE I

because of higher relative velocity. The stronger vortex will remain on this side unless an outside disturbance disrupts it. Which side of the cylinder the stronger vortex forms on first is a matter of random disturbance or fluctuation. The probability is equal in a symmetric system of either side getting the stronger vortex. The point is that when one side gets the bigger vortex it keeps it from cycle to cycle. Figure 1 also illustrates what happens above K of 15. Two vortices or more are shed at higher values of K. At K of 15, two vortices are shed and symmetric forces occur because a vortex is on each side to add relative velocity to the flow in each half cycle.

Sarpkaya found that C_m, the inertia coefficient, was assymptotic to 1.75 at higher Reynolds numbers. C_d, the drag coefficient, is asymptotic to 0.62.

Less seems to be known about transverse or lift forces than in-line forces. Sarpkaya investigated the lift forces as well as the in-line forces. According to his work, lift forces can be of the same order of magnitude as the in-line forces. More important than the order of magnitude of the forces is the frequency of occurence of these forces. Lift or transverse forces are caused by the development and shedding of the vortices in the low pressure area behind the

cylinder. A basic force imbalance occurs. When the two vortices grow at different rates, lift occurs. The instantaneous lift force resultant is in the direction of the stronger vortex due to the pressure being lower in that region. When a vortex is shed finally then the opposite side has the larger vortex and lower pressure and in steady state the situation is cyclic and given the name "Von Karman Vortex Street." In a reversing flow field, the same phenomenon can occur initially and will yield a force that varies with time.

Sarpkaya's test chamber was a U-tube 6 feet by 3 feet on the vertical legs and constricted to 3 feet square at the horizontal test section. The test cylinders had been given 1/32 inch end clearance from the side of the test section. Sarpkaya reports that flow in the test section is uniform. Neither sufficient time nor length for boundary layer development on the test section walls exists according to Sarpkaya. Also, blockage has no effect in his experiments on the readings for the same reasons. The period of oscillation was 5.772 seconds, the natural period for the water oscillation in the U-tube.

The amplitude of oscillation was held at the desired level by synchronizing air pressure at the same frequency as the natural frequency of water oscillation in the U-tube.

The cylinders were mounted to the test section by means of force transducers to self aligning bearings at the sides of the U tube. The results were correlated to Keulegan and Carpenter Number:

$$K = \frac{U_m \tau}{d} \tag{2}$$

and

$$\beta = \frac{d^2}{\nu \tau} \tag{3}$$

where U_m is maximum velocity, τ is period, d is cylinder diameter, and ν is kinematic viscosity. β is actually the Reynolds number divided by the Keulegan-Carpenter number. The nondimensional parameters above in (2) and (3) are developed from the following dimensional analysis:

$$\frac{F}{0.5\,\rho d\, LU^2} = \Phi\left(\frac{U\tau}{d},\ \frac{Ud}{\nu},\ \frac{t}{\tau}\right) \tag{4}$$

$$= \Phi\left(K,\ R,\ \frac{t}{\tau}\right) \tag{5}$$

where F is force, ρ is fluid density, L is cylinder length, t is time and d, U, τ and ν are as defined for equations (2) and (3). U_m may be substituted for U as it was in (2), in which case the equations refer to maximum velocity.

Equation (3) was developed to remove the redundance of U in both K and R. It is simply R divided by K. The cylinder used in the U tube ranged from 1.99 to 6.475 inches in diameter. Blockage ratios of diameter divided by test

section width ranged from 0.055 to 0.18. Values of the lift coefficient were measured by Sarpkaya and were found to vary from a low of 0.12 to a high of 3.9.

Isaacson and Maull [4] measured transverse forces acting on cylinders subjected to wave action. Their cylinder is mounted to a rigid platform which spans a wave tank that is 58.5 feet long, 1.9 feet wide and up to 2.6 feet deep. A pebble beach absorbed waves generated by an oscillating paddle at the opposite end of the tank. The forces were correlated to K and R. The dependency on R is not as strong as on K for $R < 20{,}000$. As R becomes larger, the force coefficients become more a function of it. Different values of the wave depth parameters $kh = 2\pi\, h/\lambda$, where h is height and λ is wave length were used. Values of

$$C_{L,rms} = \frac{F_{rms}}{0.5\ \rho d L U_m^2} \tag{6}$$

where all terms are as defined previously and F_{rms} is the root mean square value of the force were found to range to 1.1 and the semi-peak values of the coefficient ranged to almost 1.8, peaking at $K \cong 10$.

Sarpkaya also found a lag between peak force and velocity. Peak force was developed after peak velocity had been reached and velocity of the fluid relative to the

cylinder was actually decreasing. This happens because it takes a finite amount of time at a given R value to develop the flow or, in this particular case, the vortex. In perspective with a steady flow analysis, we have many different cases of the starting condition approaching a given steady state R value. Just as R peaks, velocity decreases instead of remaining at the maximum value. Therefore, the strength of the vortex is not as great as it would be with R at steady state. The vortex will continue to increase its strength until it equals the now decreasing Reynolds number, unless it gets strong enough to shed.

Heinzer's [3] investigation with the aid of a high speed camera verified and collaborates most of the quantitative findings of the nature of vortex shedding in an oscillating flow field. Heinzer observed several interesting features.

Along with the normally primary vortex there is a secondary vortex formed. This is shown in Figure 2. It is bounded by and fed by the primary vortex. It is also bounded by the shear layer and the cylinder itself. When the relative velocity of cylinder to fluid changes direction, then two vortices are pushed out of the way. The primary and secondary vortices are of opposite rotation.

Heinzer also found that once the cylinder velocity had peaked, the vortices were still growing to some extent.

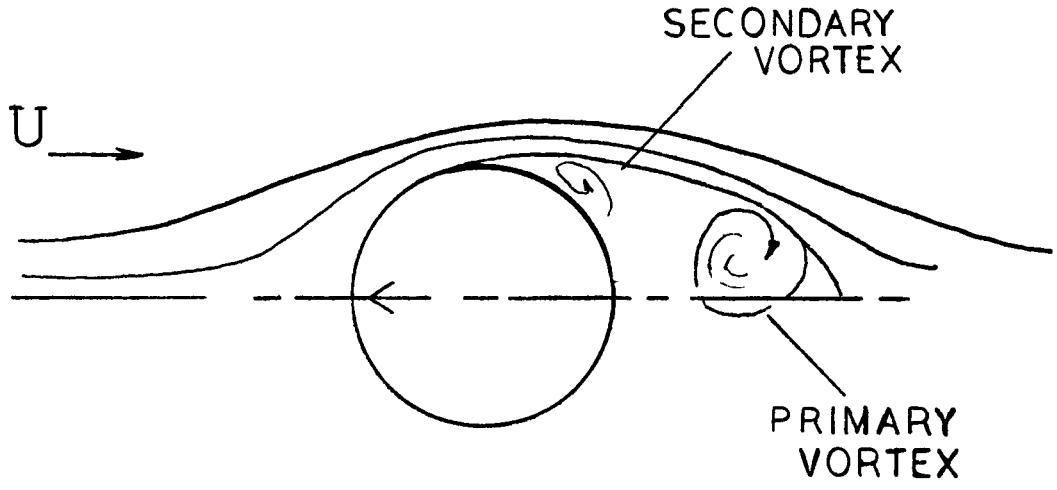

SECONDARY VORTEX FORMATION

FIGURE 2

Sarpkaya observed the same thing. This is because even though R is decreasing it still has a higher value than the corresponding steady state value for the vortex. There is still an imbalance, and separation and back flow leading to vortex formation are still present. Measurements by Heinzer indicate that the vortex may triple its size over that size it had when velocity reached a maximum.

Heinzer also noted that at a given K or $U_m \tau/d$, which is also 2π a/d, where a is amplitude of oscillation the, pattern did not change. Isaacson and Maull found this also. Whatever the given K value, frequency or speed did not seem to change the visible flow pattern much. As velocity increases, the number of cycles needed to attain a fully "disturbed" flow field near the cylinder is less. The range of oscillation frequencies of the cylinder wave from 1 Hz down to 0.25 Hz yielding values of U_m from 36 in/sec down to 9 in/sec. Values of K ranged from 30.14 down to 2.5 in Heinzer's tests.

Another interesting feature of all of the workers surveyed was the randomness in the data. Sarpkaya states that a statistical method may be needed to obtain more complete information. Hunt initially attempted measurement of transverse forces but reported that the signal was too "spurious" from the strain gage transducer.

Isaacson and Maull used an elementary averaging technique yielding average lift coefficients. The present work is an extension of the work of Isaacson and Maull and Sarpkaya.

An attempt is made to study frequency or time-variant characteristics to determine what the excitation frequencies are due to fluctuating lift. What the amplitude of the time-variant force coefficient is also is of interest. Information about fatigue forces from the alternating lift should be gained.

Isaacson and Maull used a wave tank and generated waves. Sarpkaya held his cylinder fixed in a relatively narrow conduit and oscillated the water. In the present investigation the water is at rest in a relatively very large tank and the cylinder is oscillated with simple harmonic motion. Isaacson and Maull had some small lengthwise variation in velocity due to the attenuation with depth of the water particle velocity. There should be almost none in these tests due to the lack of surface effects.

CHAPTER 2

EXPERIMENTAL APPARATUS

These tests were carried out in a wave tank. The tank dimensions are 10 feet wide by 6 feet deep. The tank is 82 feet long when the wave-making paddle and beach section are discounted. The entire apparatus was suspended over the water with two composite wood beams made of four 2 by 6's each. Wood was chosen because of economics and its good damping characteristics. Simple harmonic motion was generated by means of a scotch yoke mechanism. The scotch yoke mechanism was suspended from the wooden beams by a frame made of 3 inch channel iron. The yoke consists of a guide-piece with a milled slot. The guidepiece is fastened to chrome rods that ride in linear ball bearings. The arm of the yoke is driven by a pulley and belt from a variable speed DC motor through a bevel gear drive. The arm is fitted with a slider block which can be adjusted to control the stroke. It was essentially the same yoke as used by Hamann [11] and Hunt [2] and is shown in Figures 3 and 3a.

Initially the work was attempted in a smaller tank with water volume dimension of 8 feet long, 2 feet wide and 1.5 feet deep. The test cylinder is 2 inches in diameter.

SCOTCH
YOKE & DRIVE

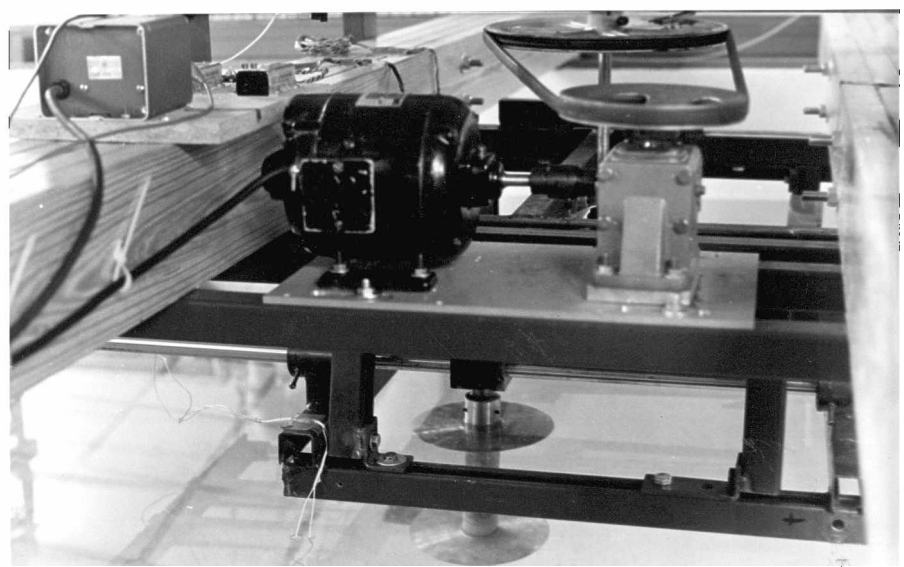

FIGURE 3

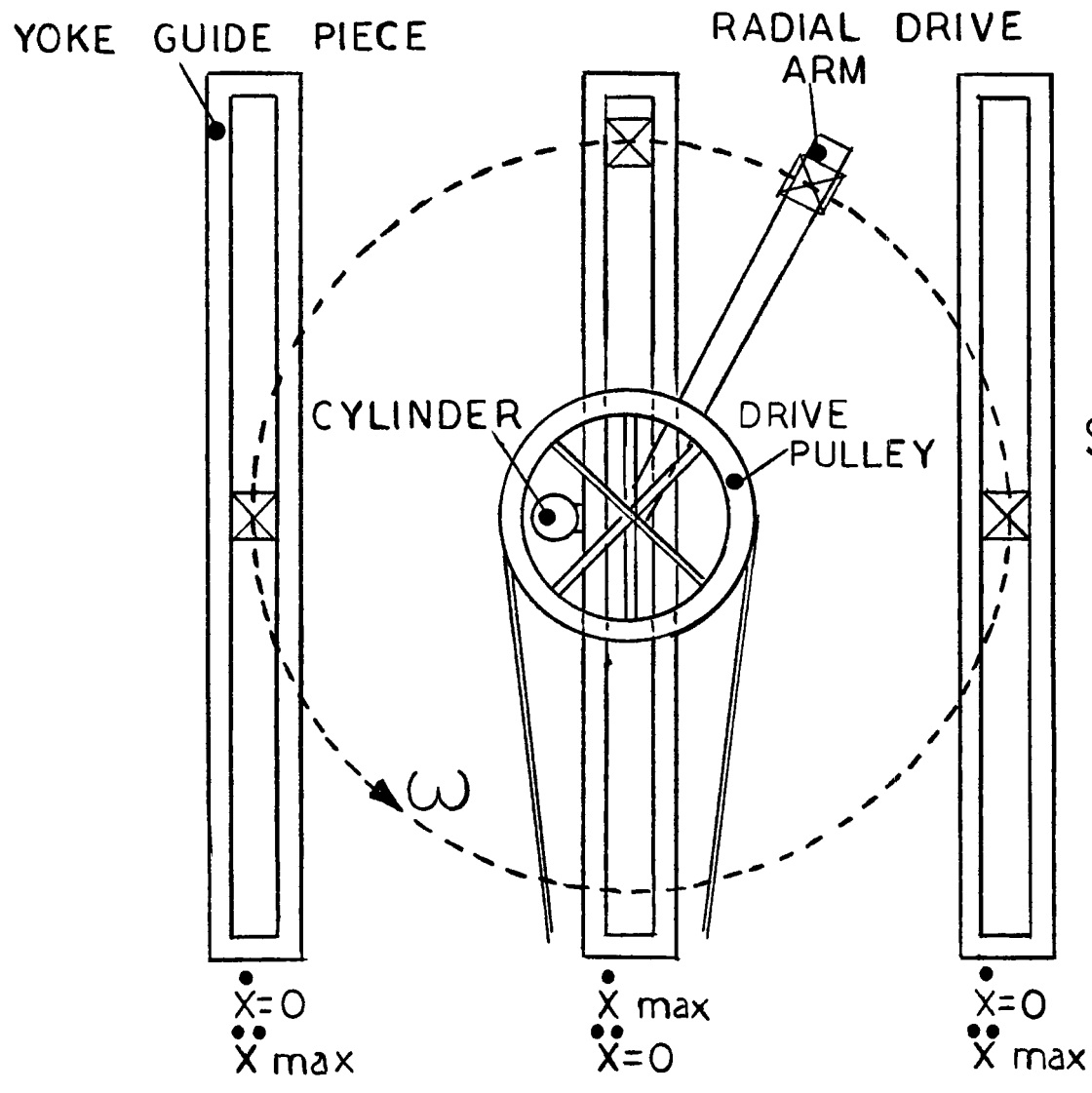

SCOTCH YOKE
FIGURE 3A

Although the blockage ratio of cylinder diameter to tank width was less than 0.010, the flow was dominated by secondary effects. The most serious secondary effect was the sloshing of the tank itself. The predominant standing wave had an amplitude of just over 4 inches and a wave length, λ, of about 16 feet. Other effects such as wake reflection from the sides could be seen but were not measured in the small tank. In the large wave tank, a capacitance wire type depth gauge was calibrated and used to measure surface effects generated by the motion of the cylinder in the final test. The gage was placed 45° from the direction of travel of the cylinder and 18 inches from the center of cylinder travel.

Design of the Transducer Beams

Previous work indicated that the use of a single cantilever strain gage beam was not very satisfactory. It gave nonuniform deflection along the length which would vary results spanwise. The deflection is greatest at the cantilever tip farthest from the strain gages. The previous design was simply a cantilever rectangular cross section aluminum beam. It was fastened to the carrier bracket on the yoke at the top and the top of the cylinder on its lower end. Two gages, one on each side, were mounted and their strains summed in a Wheatstone bridge. These gages were self

compensating for temperature and 120 Ω nominal resistance with a gage factor of 2.01.

In order to keep the far tip at the bottom of the cylinder from moving outside the theoretical boundary layer, insufficient strain was produced at the gage area to get good response. Steady state values for the boundary layer displacement thickness were used [5]. This is because no information on the boundary layer could be found in the literature for oscillating flows.

In order to solve this problem, the test model shown in Figure 4 was built. This arrangement uses two cantilevered transducer beams mounted to a rigid 1-inch pipe at the fixed end and supported by ball and socket joints at the test cylinder. The active test cylinder was contained in the center of the configuration. Self-compensating gages designed for aluminum were fastened to the beams as near the fixed end as possible. The gages were 350 Ω with a gage factor of 2.11. Semi-conductor gages were considerd but the cost was prohibitive.

Several beam configurations were investigated. Deflection at the mounting point to the cylinder, the end of the transducer beam, should not exceed 0.010 inch at the maximum expected loading. Unfortunately, the value of maximum

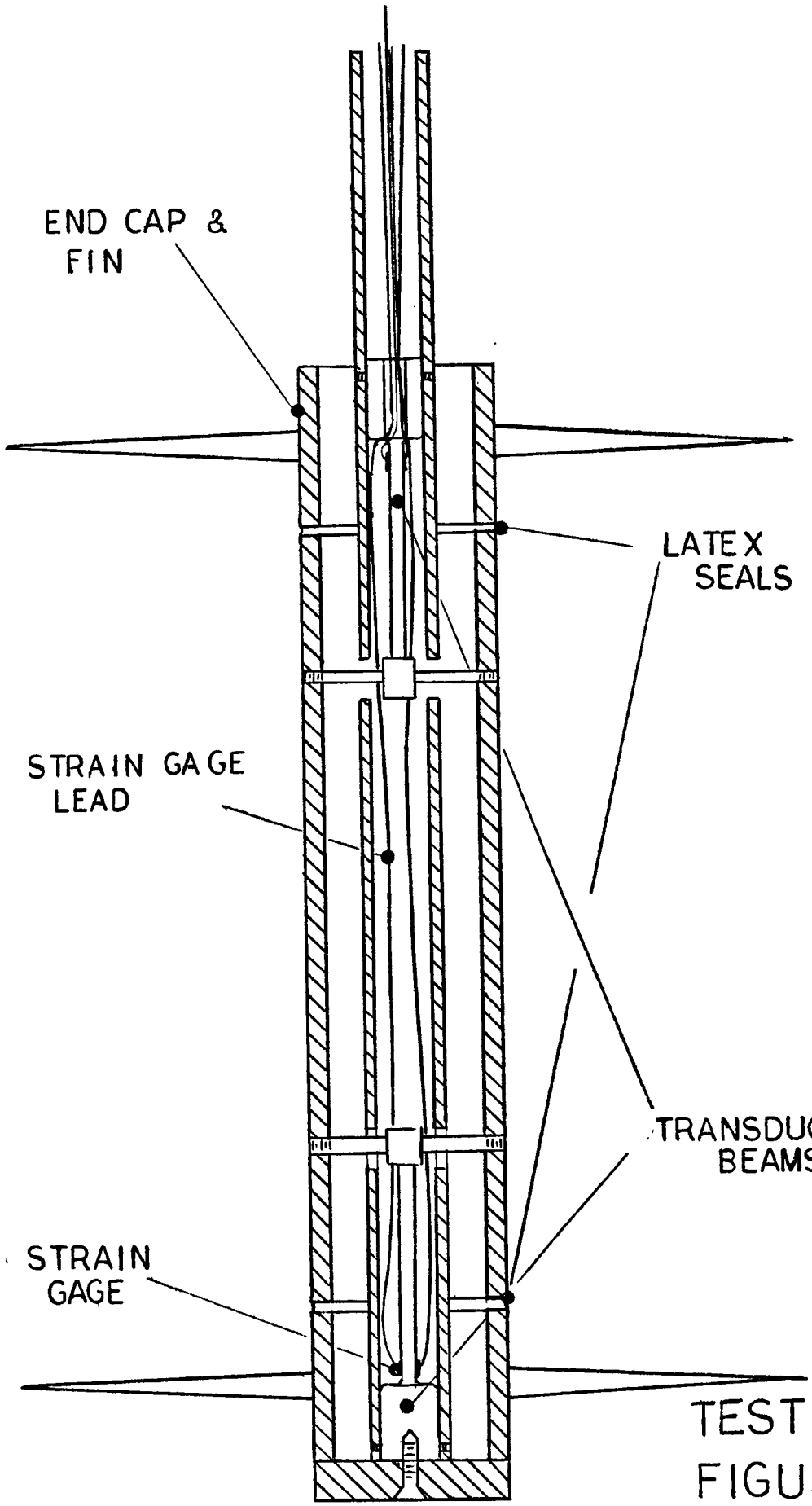

TEST MODEL
FIGURE 4

deflection was due to considering a steady state boundary layer displacement thickness. It is more likely that the boundary layer is not as thick as steady state due to lack of time for development - especially at higher R in the test. An I-beam cross section was first investigated. It proved impractical even though strain would be high in the flange with minimum deflection because the flanges would be much too thin and frail. The final design was a simple rectangular cross section. The deflection, Δ_{max}, was calculated from the following:

$$\Delta_{max} = \frac{FL^3}{3EI} \quad , \tag{7}$$

where F is force, L is length, E is Young's modulus, and I is the moment of inertia. This is the linear deflection equation for a cantilever beam at the free end.

The gain or strain is found by relating stress to strain to gage factor as follows:

$$\sigma = \frac{MC}{I} \tag{8}$$

where σ is stress, M is moment, C is the distance to the neutral axis. The strain is

$$\epsilon = \frac{\sigma}{E} \quad , \tag{9}$$

so

$$\epsilon = \frac{F\,L\,C}{E\,I} \tag{10}$$

relates gain to force since

$$\epsilon = G.F./\Delta R/R \tag{11}$$

where G.F. is the gage factor and R is resistance of the gages.

Equations that relate strain and gage factor to voltage change in the bridge are not needed since the beams were conveniently compared to the old single beam design. By comparison, the new beam was properly sized.

The values of deflection and strain were estimated using 1 lb_f per beam for a relative maximum force. The following values were obtained for the beam in Figure 5. This beam is 4 inches long and has a cross section of 0.370 inch by 0.125 inch thick,

$$\Delta_{max} = 0.0117 \text{ inch} \tag{12}$$

$$\epsilon_{max} = 478\ \mu\epsilon \tag{13}$$

Both of these values were thought satisfactory. Since there would be two beams and 4 gages, 2 lb_f could be carried and the gain would be quadrupled without excessive deflection.

Since the system was going to be used to measure parameters that are strong functions of time, the system response was also considered. During design, a lumped parameter model was used to calculate the expected natural

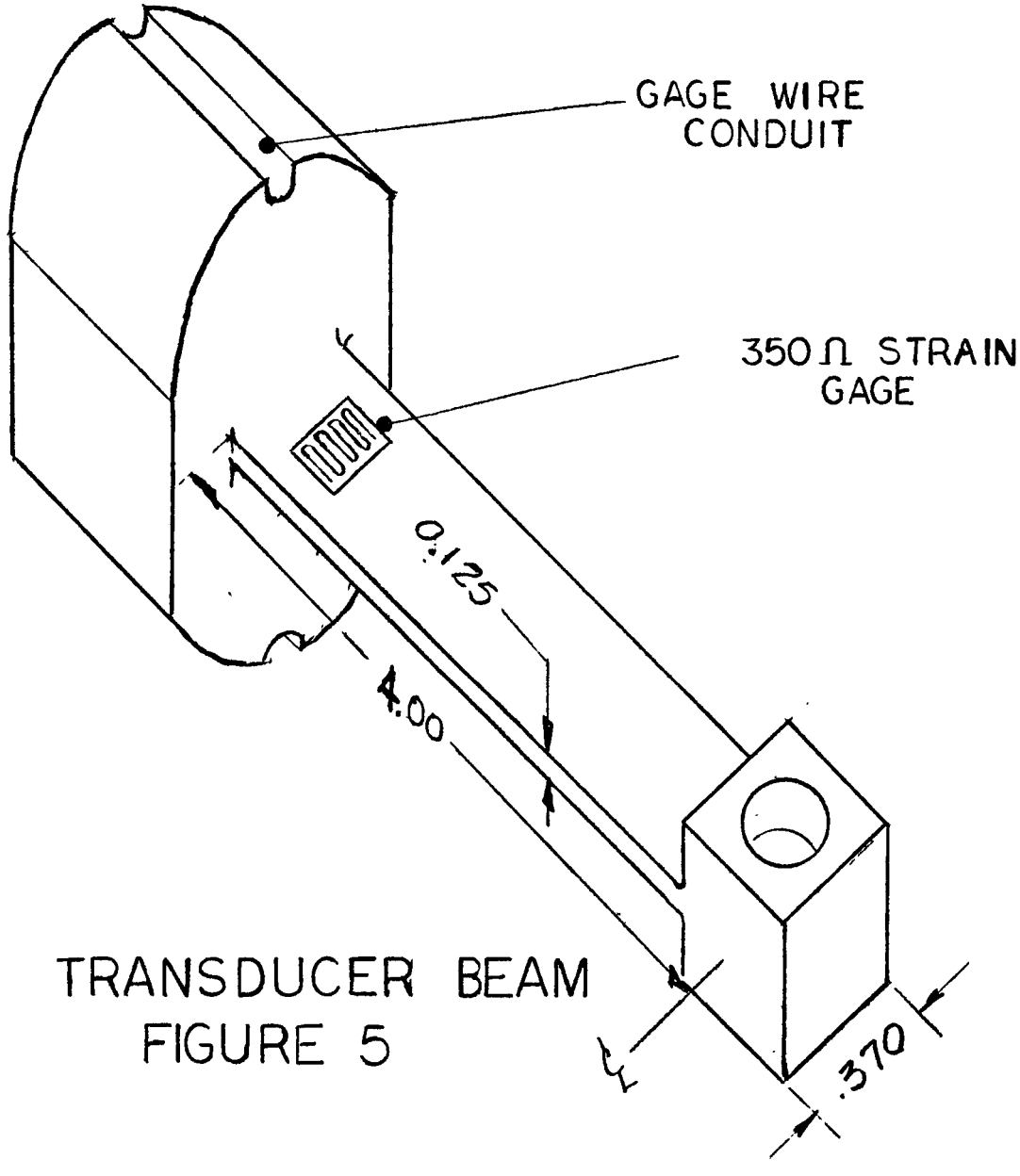

TRANSDUCER BEAM
FIGURE 5

frequency. Then the frequency was measured by thumping and by displacing the cylinder in water. The value of the system-damped natural frequency in water is 14.7 Hz. In order to prevent resonant oscillations, the desire was to get the frequency ratio

$$\frac{\omega_f}{\omega_n} \quad , \tag{14}$$

where ω_f is forcing frequency and ω_n is natural frequency, as close to zero as possible. For linear, second-order systems, this would produce a dynamic magnification factor of nearly 1.0 or give no gain to the mechanical signal. We did not want the test model to become a mechanical oscillator. With the exception of the latex rubber seals, the system is linear. Tests showed that the seals had an increased effect at the lower deflection estimated at 5% change in force vs. voltage on the model when they were in place.

With the natural frequency at 14.7 Hz and the maximum expected frequency expected to be about 3 Hz, the ratio in (14) was 0.20. This was not expected to be a problem. Phase shift was almost negligible at less than 3% calculated.

Actual measurement, as discussed in the data reduction section, of this system's dynamic properties showed excellent characteristics.

Beam material was 6061-T6 aluminum alloy. This alloy was chosen because of weight, (desire to keep rig inertia forces low), high yield strength (40,000 psi), corrosion resistance and machinability. Tolerances were measured at ±0.003 inch on the thickness taken lengthwise and ±0.001 inch on the width taken lengthwise. Both waterproof and oilproof gage coats were used. The gage mounting area was polished mirror smooth before roughing back for mounting.

The Total Cylinder Model

The test model was designed to similate the leg of an offshore platform or any uniform diameter cylinder. The end caps with fins were used to minimize end effects - make the cylinder infinite in length so to speak. An inside cylinder of schedule 80, 1-inch diameter steel pipe was used to "carry" the entire model assembly. The top of the steel pipe was mounted to a bracket attached to the yoke.

The fins on the end caps were made from 6061-T6 aluminum, cut on a taper and polished mirror smooth. They are 10 inches outside diameter and have an undersized 2 inch hole in the center. The fins were shrink fitted to the caps at about 0.005 inch interference fit.

The caps and the cylinder were finished smooth at 2.000 ± 0.010 inches outside diameter. The live test

section is 13.370 inches long. The inside pipe was bored to 0.002 inch over the outside diameter of the transducer beam's big ends. The beams were positioned in the steel pipe and clamped rigidly with set screws after the cylinder live section was mounted and aligned with its pins fastened to the socket end of the transducer beams. The pins mounting the live section to the transducer beams were 1 inch long 10 x 32 screws. The screws were ground round and slotted on the opposite end. The cylinder was drilled and tapped on a vertical mill and the screws were locked with a sealing compound and the holes sealed with wax. The sockets were filled with no. 2 grease to inhibit wear and give free action at the end of the transducer beams. After the test section of the cylinder was securely mounted, the end caps were mounted and then the rubber seals were mounted. With the rubber seals in place, a polyeurethane gage coat was used to seal them at the cylinder and end cap. The seals were latex and very sturdy but had a tendency to rot. However, calibration stayed within about 3% average whenever seals were changed. Both end caps and the cylinder were cut down by 0.005 inch in the area of the seals to accomodate both the seals and gage coat. The final assembly was given several coats of clear rust proofing enamel after all holes were filled with wax.

The deflection of the inside steel cylinder was estimated in the neighborhood of 0.001 inch using equation (1). The small clearance holes for the pins were ignored in this analysis.

Figure 4 shows the cross section of the entire assembly with the transducer beams (Figure 5), rubber seals, end caps and fins all in place. The top of the top cap is sealed to the inner pipe with nitrile rubber to prevent water leakage.

Slider Crank Mechanism and Yoke

The basic mechanism, sometimes known as a Scotch Yoke, has been discussed and is shown in Hunt [2] and in Figures 3 and 3A. One slight change was made worth mentioning. The slider block itself was slightly misaligned to the yoke guide piece. By doing this, just short of binding and raising the slider halfway out of the slot, the jerk force at the ends of travel was greatly minimized. This jerk force is a step input to the system and is caused by the change in sign of the acceleration force at each end of the yokes travel. By reducing this jerk force, the amplitude of the excited natural frequency was reduced so much that 60 Hz noise was more of a problem than the 14.7 Hz "first critical" of the cylinder. The yoke guidepiece was kept well lubricated and the brass slider block on the radial arm moved freely.

Velocity Time Measurement

Previously, a contact type limit switch was used to signal the position of the yoke. This introduced a slight step input into the mechanical system. This was replaced with a noncontact eddy current probe. The probe itself is basically a coil and is driven by an amplifier with a carrier frequency in the megahertz frequency range. When the field from the probe is interruped by a conductive ferric material, like steel, a back EMF voltage is produced which is linearly proportional to the distance from the probe. The fact that it is noncontact makes it very useful since it causes no mechanical interference. The probe driver is set up using negative 18 volt power supply. The voltage is very critical to calibration and when the system is properly balanced it is dynamically flat up to the Kilohertz range.

Instrumentation Subsystem

The instrumentation subsystem consisted of a Bridge Amplifier (Wheatstone bridge and D.C. Amplifier) in a self contained unit, an active low pass electronic filter, a dual DC power supply and the proximitor system. A voltmeter and oscilloscope as well as a Bureau of Standards calibrated oscillator were used to check system components periodically as well as the instrument subsystem response. Figure 6 shows

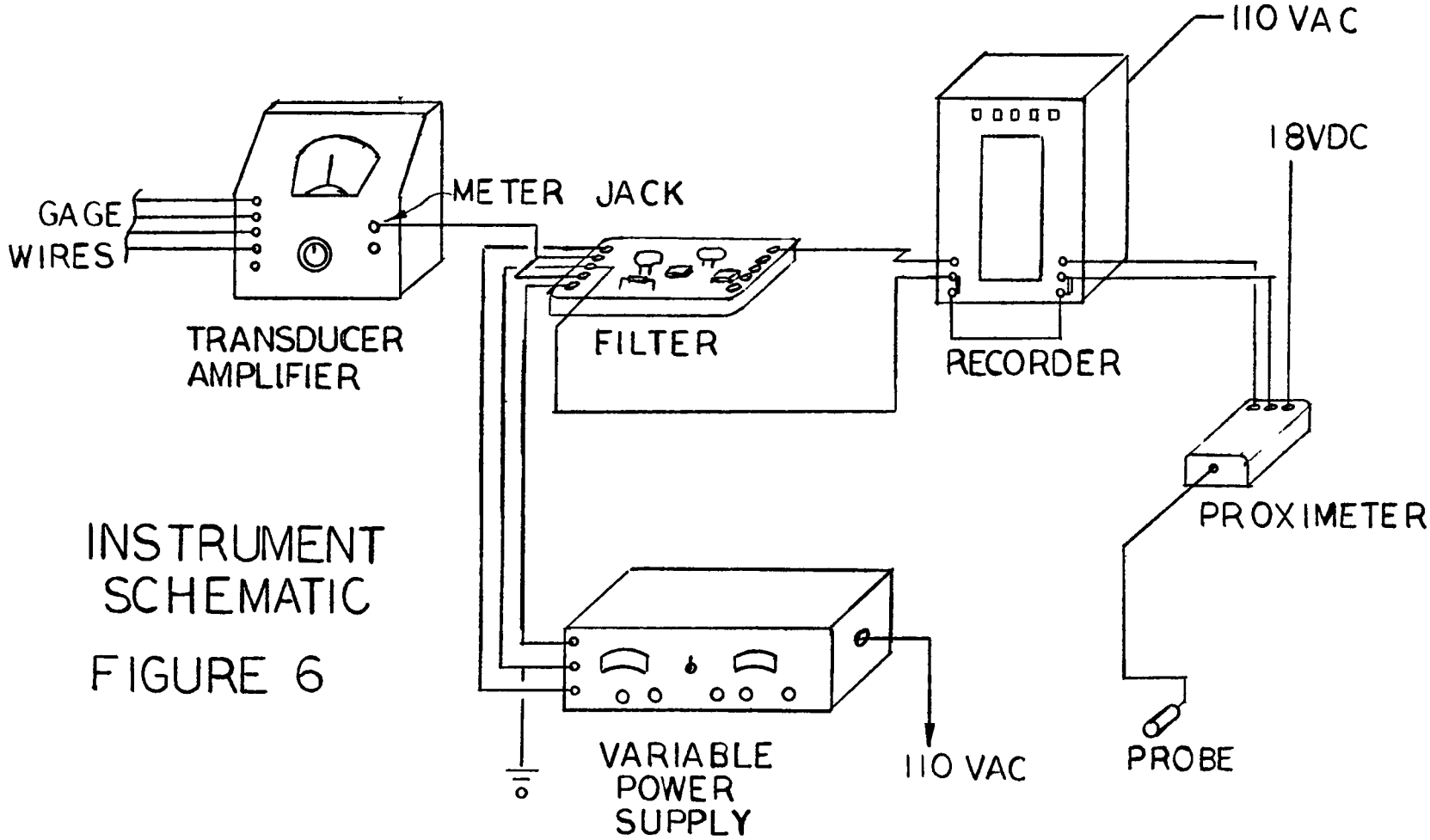

INSTRUMENT SCHEMATIC

FIGURE 6

the schematic layout of the subsystem and Figure 7 shows the electronics near the wave tank.

The bridge and D.C. amplifier unit has a linear range of ± 5 volts with a 100 KΩ load or more and ± 0.5 milliampere with a 1 KΩ load. The actual load was the 10 megohm strip chart recorder input impedance. The unit has flat response from D.C. to 2 KHz when using the meter output jack to drive a recorder. Internal resistors were available and could be switched into the bridge to check the calibration of the amplifier output gain. Sensitivity of the unit was ± 25 με up to 2000 με with 350 Ω strain gages.

The active electronic filter was designed specifically for this research. The natural frequency of the cylinder due to jerk force excitation was a problem and needed blocking. Bearing noise from the rolling element linear bearings guiding the yoke guidepiece and 60 Hz line noise were also problems. The intent of the design was to get as close to a maximally flat Butterworth response in the frequency domain and the fast rise time minimal overshoot Bessel response in the time domain. Actual results were quite good for the second order circuit shown in Figure 8. The frequency response is shown in Figure 9. The corner frequency is 4.9 Hz with attenuation of 16 db per

INSTRUMENTATION

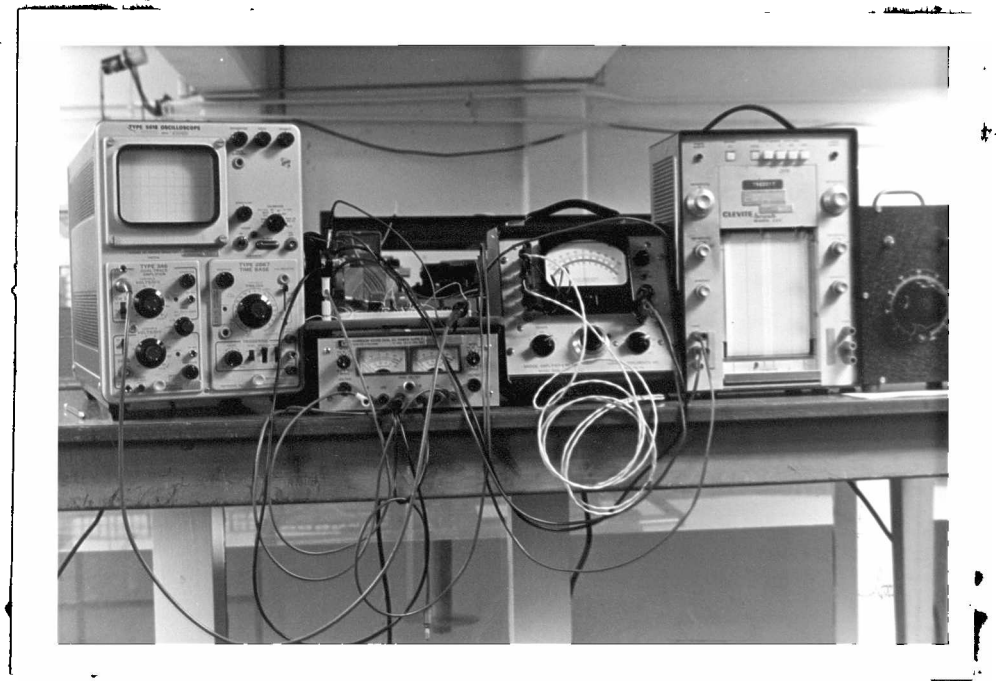

FIGURE 7

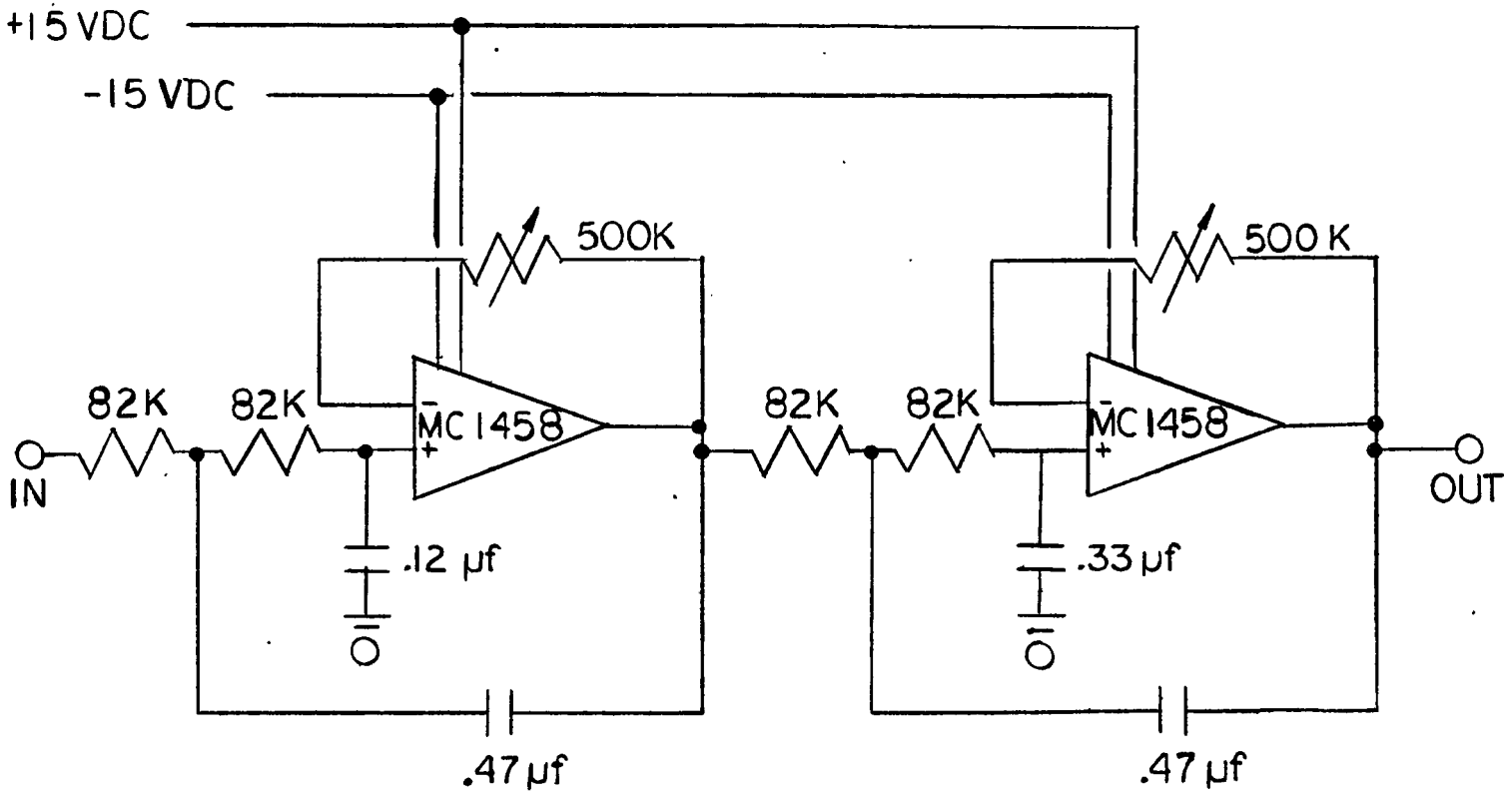

FILTER SCHEMATIC
FIGURE 8

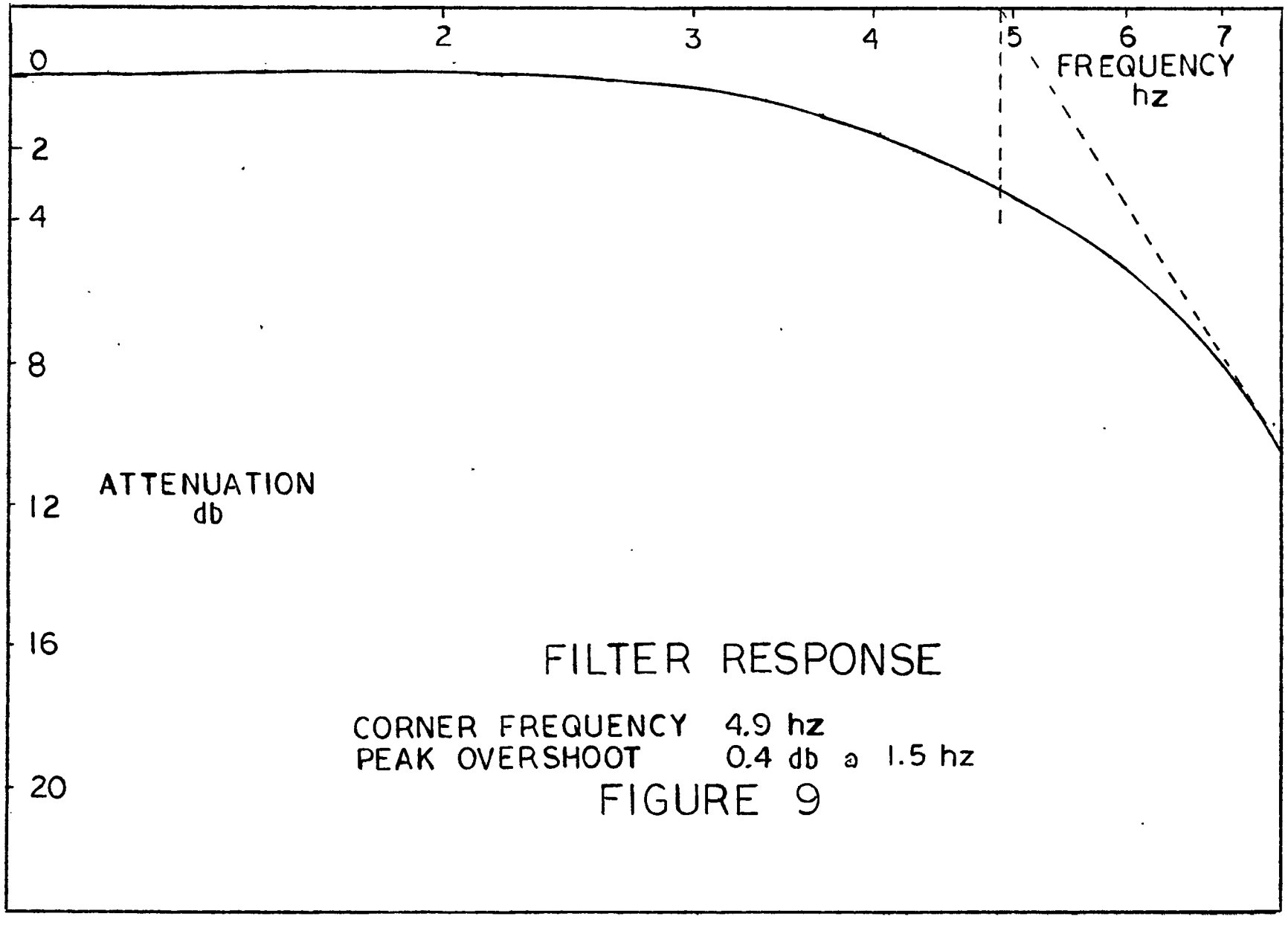

FILTER RESPONSE

CORNER FREQUENCY 4.9 hz
PEAK OVERSHOOT 0.4 db a 1.5 hz

FIGURE 9

octave. The pass band gain of the filter was 0.4 decibel at 1.5 Hz. The phase shift is shown in Figure 10. Instead of the normal plot, this plot is percent phase shift versus frequency. The phase shift plot was used to shift the velocity or displacement mark back to its real time position where it would have been had the strain gage trace not been shifted through the filter.

In the time domain, the response was observed. The rig itself was used and was both thumped and displaced to excite the natural frequency. True, this is not a fast rise square wave, but interest is not in the response for universal application of the filter but its usefulness in this research. The response is shown in Figure 11. The peak overshoot was 6% with a rise time of 0.112 second. The upper trace shows the unfiltered response or comparison.

The filter was tuned to the needed response by changing the shunt capacitor on the second stage and adjusting the 500 KΩ pots in the feedback loops. The final value of the second stage shunt capacitance was 0.33 microfarad. The filter and its power supply are shown in Figure 12. Position and timing was accomplished by using the noncontract probe described earlier in this report.

The recorder is a two-channel,pressurized ink pen instrument. It has two independent channels. The input

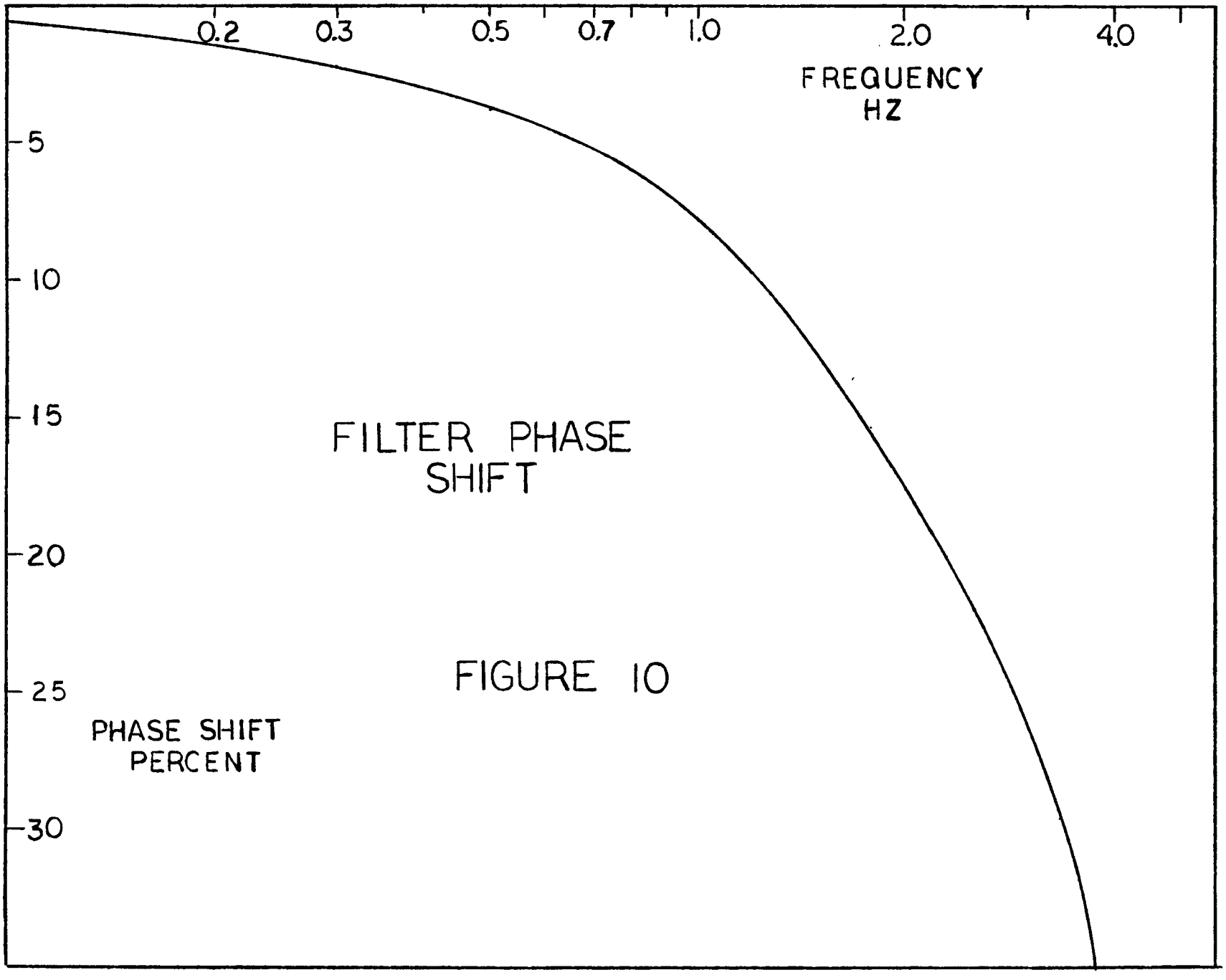
0.2
0.3
0.5
0.7
1.0
2.0
4.0
FREQUENCY
HZ
5
10
15
20
25
30
FILTER PHASE
SHIFT
PHASE SHIFT
PERCENT

FIGURE 10

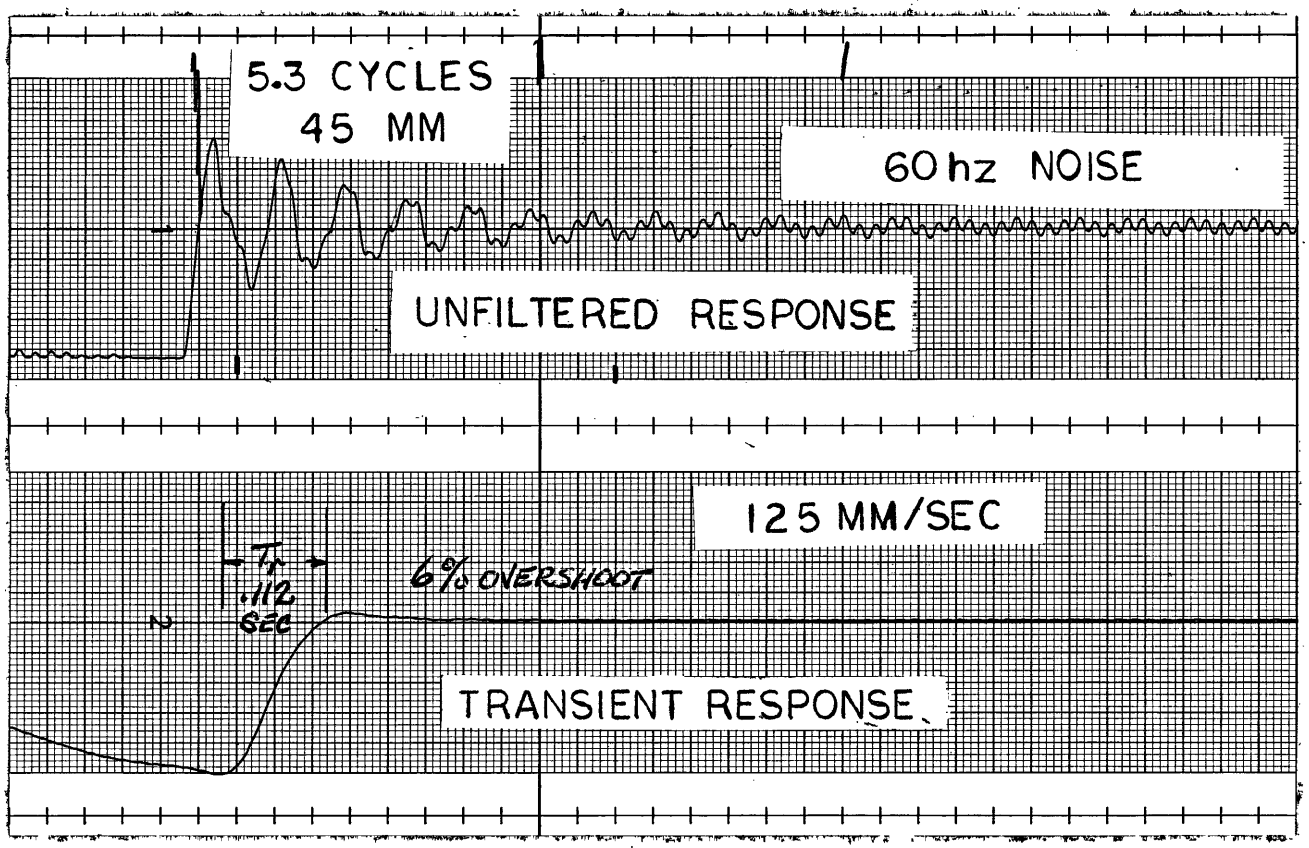
5.3 CYCLES
45 MM
60 hz NOISE
UNFILTERED RESPONSE
125 MM/SEC
T_r .112 SEC
6% OVERSHOOT
TRANSIENT RESPONSE

FIGURE 11

FILTER & POWER SUPPLY

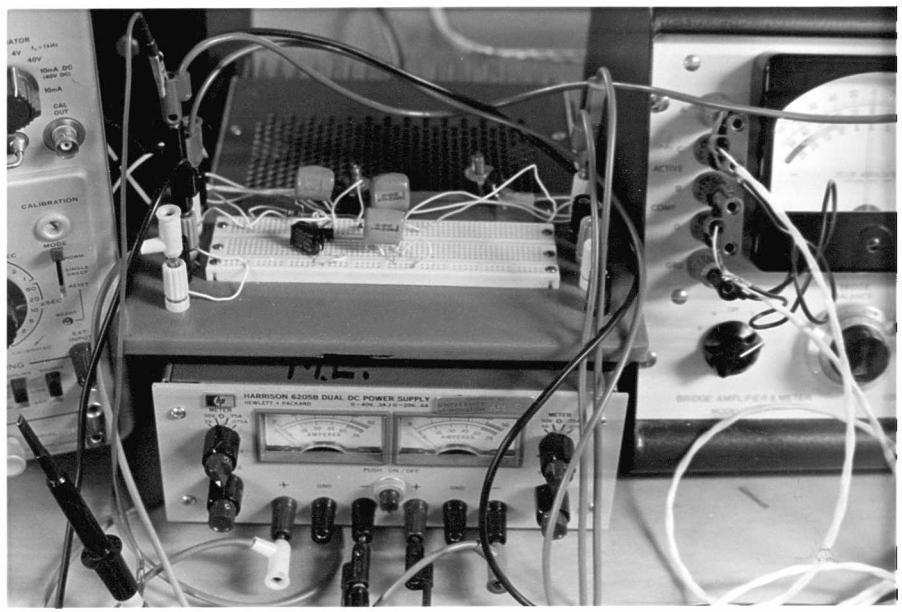

FIGURE 12

impedance is quite high at 10 megohms and response is flat to 100 Hz with 3 decibels loss coming at 125 Hz. Chart speeds ranged from 1 to 125 millimeters per second. Gain ranged from 0.001 to 5 volts.

The wave gage was a capacitance wire calibrated and found to be linear between ± 4 inch wave height. The wire is coated with polyeurethane and measures the change in capacitance with depth by the change in dielectric as water level fluctuates. The wire is in series with the primary side of a transformer driven at 2 KHz. The secondary side senses the change due to water depth. The signal is conditioned and fed to an amplifier and strip chart recorder.

CHAPTER 3

DATA ACQUISITION AND REDUCTION

Calibration of the Cylinder Model

The cylinder was calibrated in the static mode and a dynamic check was performed. Five static data points for force against strain gage output voltage were obtained for each side of the cylinder. The assumption that the force to voltage relationship would be symmetric from one side to the other was not made. In fact, there was a slight difference. The calibration proved to be very nearly linear. The difference from linearity can be explained mostly by the rubber seals and some probable hysteresis in the beams. Calibration was checked several times and found to differ by a maximum of 8% at the lower end without the seals using a digital voltmeter. With the seals left on and using only the recorder, no difference above a few percent over the entire range was seen. The recorder itself was also checked against a source calibrated to the Bureau of Standards. No measurable error was present.

The calibration curve in Figure 13 was plotted. Two power curves, one for each side of the cylinder, were fitted to the data. These curves were used in the calculation of results. The power curve used was

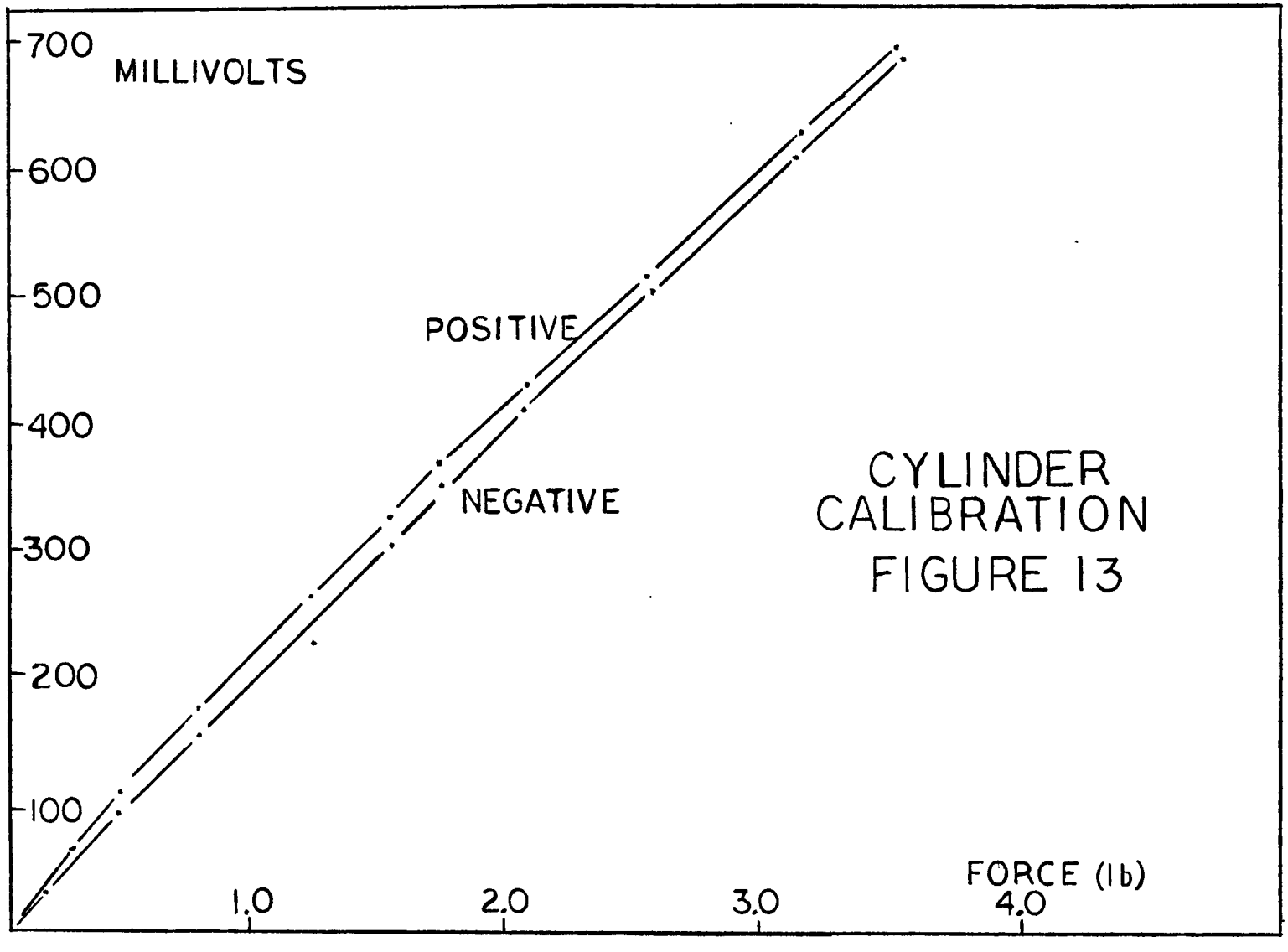

CYLINDER CALIBRATION
FIGURE 13

$$M.V. = C\ F^{b}. \tag{15}$$

where M.V. is millivolts, C is the constant, F is force and b is the exponent.

The coefficient of determination, r^2, was also calculated for each curve as a measure of goodness of fit. The positive values of voltage to force fit the following curve:

$$M.V. = 229.3(F)^{0.89} \tag{16}$$

The coefficient of determination for this curve is 0.99971. A r^2 value of 1.0 is a "perfect" fit. Negative values of voltage to force fit the following curve:

$$M.V. = 207.11(F)^{0.97} \tag{17}$$

The coefficient of determination for this curve is 0.99530.

The fact that the curves are so close to linear bears out the soundness of the rig design as long as deflections are kept small. The latex rubber seals are inherently non-linear. However, they do not provide enough restoring force to effect the curves significantly.

Calibration of the Bridge Amplifier

The Wheatstone bridge and amplifier unit was used to amplify the strain gage signal and condition it. In order to insure that the gain setting was constant throughout the testing, the same internal shunt resistance was used and the

meter was set by turning the gain knob to 830 $\mu\varepsilon$ before and after each run. The instrument had the slightest tendency to drift so constant checking was necessary.

Several minutes warmup were allowed before running any tests. The Wheatstone bridge was nulled and the amplifier was balanced. Then, the gain was set and the recorder connected to the meter jack.

Dynamic Calibration Check

The entire system was checked dynamically for response. The purpose of this was to verify that the mechanical subsystem, electronic filter subsystem, bridge amplifier and recorder were sufficiently linear in combination and separately to substantiate the results obtained.

Figure 14 shows the test schematic for the basic set-up. Initially, the system was checked without the filter. Then the filter was inserted in the system. The filter is not shown because of space limitations on Figure 14, but it is installed just as indicated on Figure 6.

The platform for the calibration was made of standard 2 inch dimension lumber. This would prevent damage to the fins and allow them to bite into the wood for a more secure mounting. The cylinder was strapped into place and wedged at the fins against rotation. The natural frequency in air

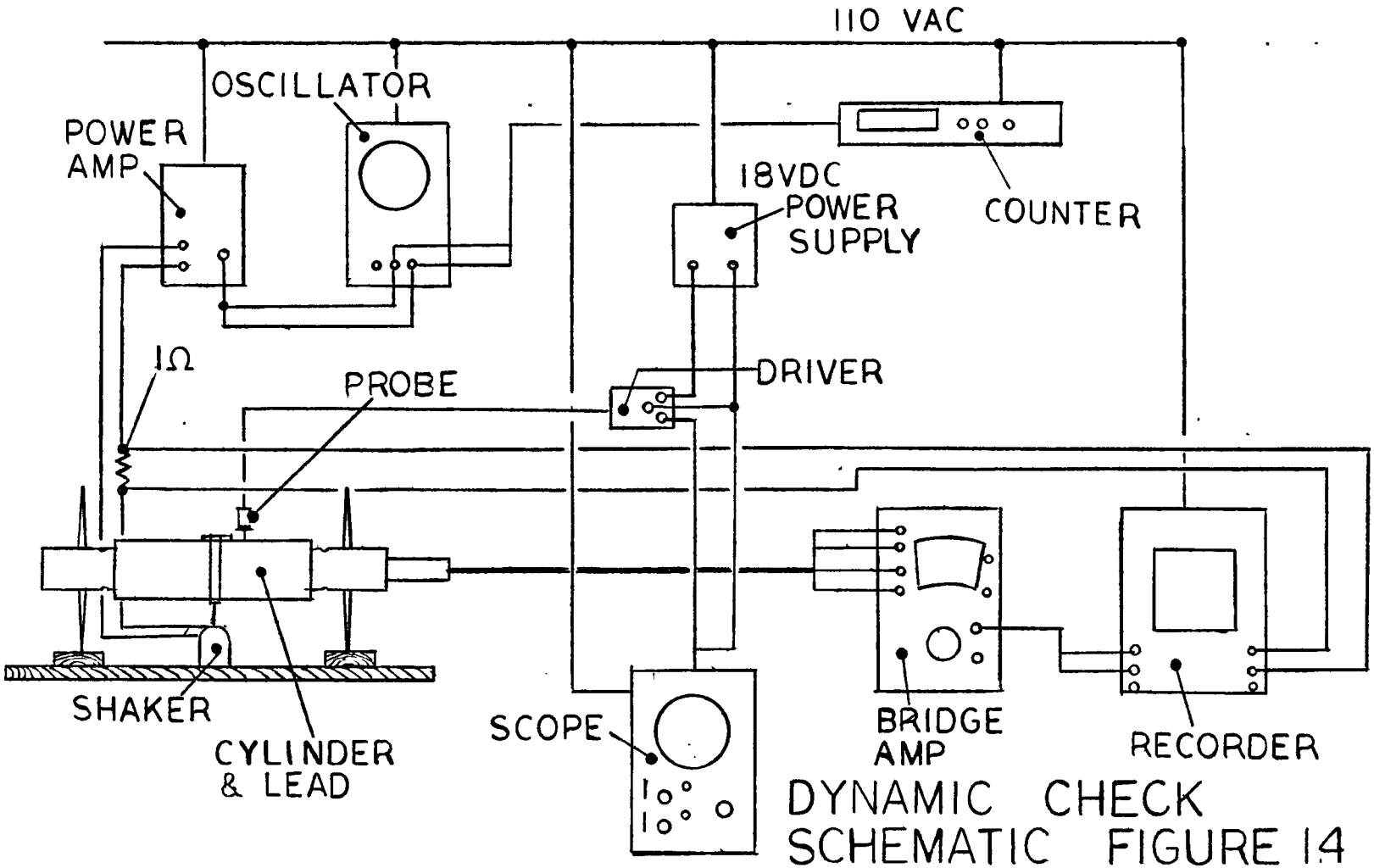

DYNAMIC CHECK SCHEMATIC FIGURE 14

was measured by thumping to be 34.09 Hz. Since the damped natural frequency in water was 14.7 Hz, mass was added to decrease the natural frequency of the cylinder. A sheet of lead was used and a test frequency of 15.4 Hz was finally obtained. A small shaker capable of yielding 2 pounds force was attached to the wooden mounting platform with small bolts passing completely through the wood. The shaker was fastened to the cylinder by using a hose clamp strapped around the lead sheet which was rolled on the cylinder. The displacement of the cylinder was monitored using a calibrated proximitor system of the same type used to measure the timing of the yoke travel. The probe was placed over a steel thumb tack pressed into the lead. The probe voltage output is linear with displacement in the range used and is dynamically flat in response up to several thousand cycles per second.

The output of the electromagnetic shaker was held constant by monitoring the current supplied to it using a 1 Ω resistor in one of the leads from the power amp to the shaker. The power amp was supplied with a sine wave signal from an oscillator which was verified with a frequency counter. The strain gages were connected to the bridge amplifier unit and this signal recorded on the strip chart

recorder. The voltage drop across the 1 Ω resistor to the shaker was placed on the other channel of the recorder and held constant.

An oscilloscope was used to monitor the output signal of the proximity probe and verify the wave form output. The proximity probe system and strain gage system were compared from D.C. up to 20 Hz and found to agree both qualitatively in wave shape and in magnitude. Both were checked statically by adding weight and a calculation shown below was performed to verify that reading force from the gages and probe yielded no difference.

The equation of motion for the system can be written simply as

$$F = m\ddot{x}\ II, \tag{18}$$

where F is force, m is mass, $\ddot{x}$ is acceleration, and II is the normalized impedance term of the system. This is only for the translation mode. In the case of simple harmonic motion, the acceleration is

$$\ddot{x} = -a\omega^2 \sin(\omega t + \phi), \tag{19}$$

where a is amplitude, ω is circular frequency, t is time and ϕ is phase angle.

The maximum value of acceleration is $a\omega^2$ where $II \cong 1.0$ at low frequencies.

So,

$$F_{max} = m\, a\omega^2 \ , \tag{20}$$

or

$$F_{max} = m\, a(2\pi f)^2 \ , \tag{21}$$

where f is harmonic frequency. The following values were obtained for the system,

1.) 300 mv at f = 1.1 Hz from the probe,

2.) 135 mv at f = 1.1 Hz from the strain gage.

We can represent the maximum force in excess of the effects of gravity from equation (21). Total weight of the cylinder, lead, clamp, and thumb tack was found to be 7.67 lb. The calibration slope for the probe was 186.94 millivolts per thousandths of an inch. So, the measured millivolt reading yields a dynamic force of 0.59 lb_f. To compare this dynamic measurement with a static load, an additional 200 gms (0.4405 lb_m) was placed on the cylinder in a static condition. The additional measurement in excess of gravitational force was 230 millivolts. Thus, the ratio of static to dynamic loadings is 0.7466 for the force ratio and 0.7690 for the millivolt ratio. The two values are within 3%.

Using the average calibration curve for the strain gage of

$$F = \left(\frac{MV}{217.73}\right)^{0.93} \tag{22}$$

where F is force, and MV is millivolts, the following is obtained

$$F = \left(\frac{135}{217.73}\right)^{0.93} = 0.598 \text{ lb.} \tag{23}$$

The difference here is

$$\frac{0.598}{0.590} = 1.013 \quad \text{or } 1.3\% \text{ increase.} \tag{24}$$

Several things are worth noting. First, the impedance term is set equal to 1 because Figure 15 verifies that this is the case at f = 1.1 Hz. Second, the calculations and curves were not normalized because the objective was only to verify calibration. Third, gravity was left out of the force calculations for the same reasons as above.

The last step in the procedure was to put the filter in the system and check response of the cylinder, filter, bridge amplifier, and recorder all together in the frequency domain. This has been shown in Figure 11 for the time domain except that the cylinder was in water and in these tests it was mass damped. Figure 16 shows the results to be quite satisfactory.

The conclusion is that the systems are linear in the range of measurement and that static and dynamic calibration are equivalent in this range.

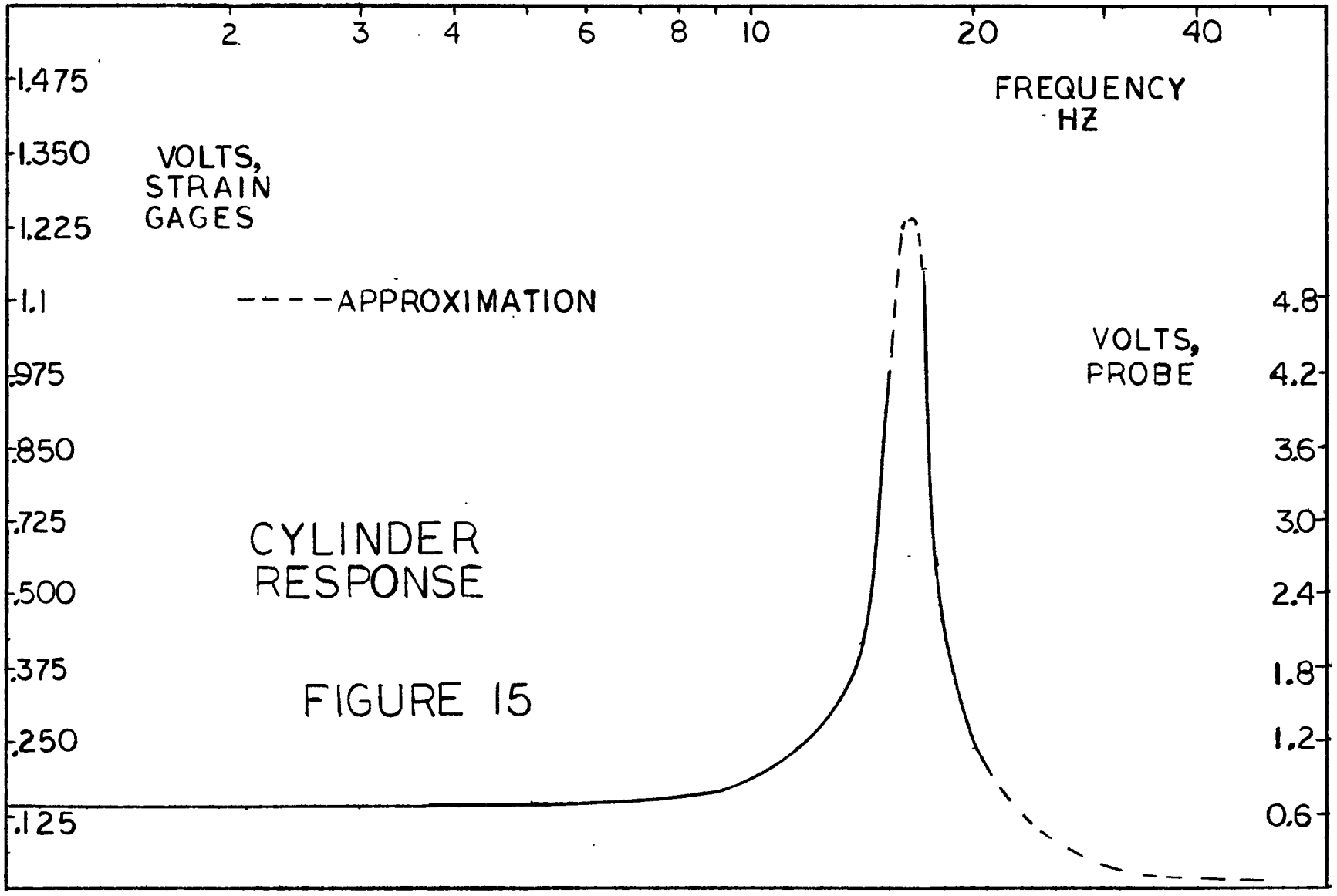
2
3
4
6
8
10
20
40
FREQUENCY
HZ
1.475
1.350
1.225
1.1
.975
.850
.725
.500
.375
.250
.125
VOLTS,
STRAIN
GAGES
----APPROXIMATION
VOLTS,
PROBE
4.8
4.2
3.6
3.0
2.4
1.8
1.2
0.6
CYLINDER
RESPONSE

FIGURE 15

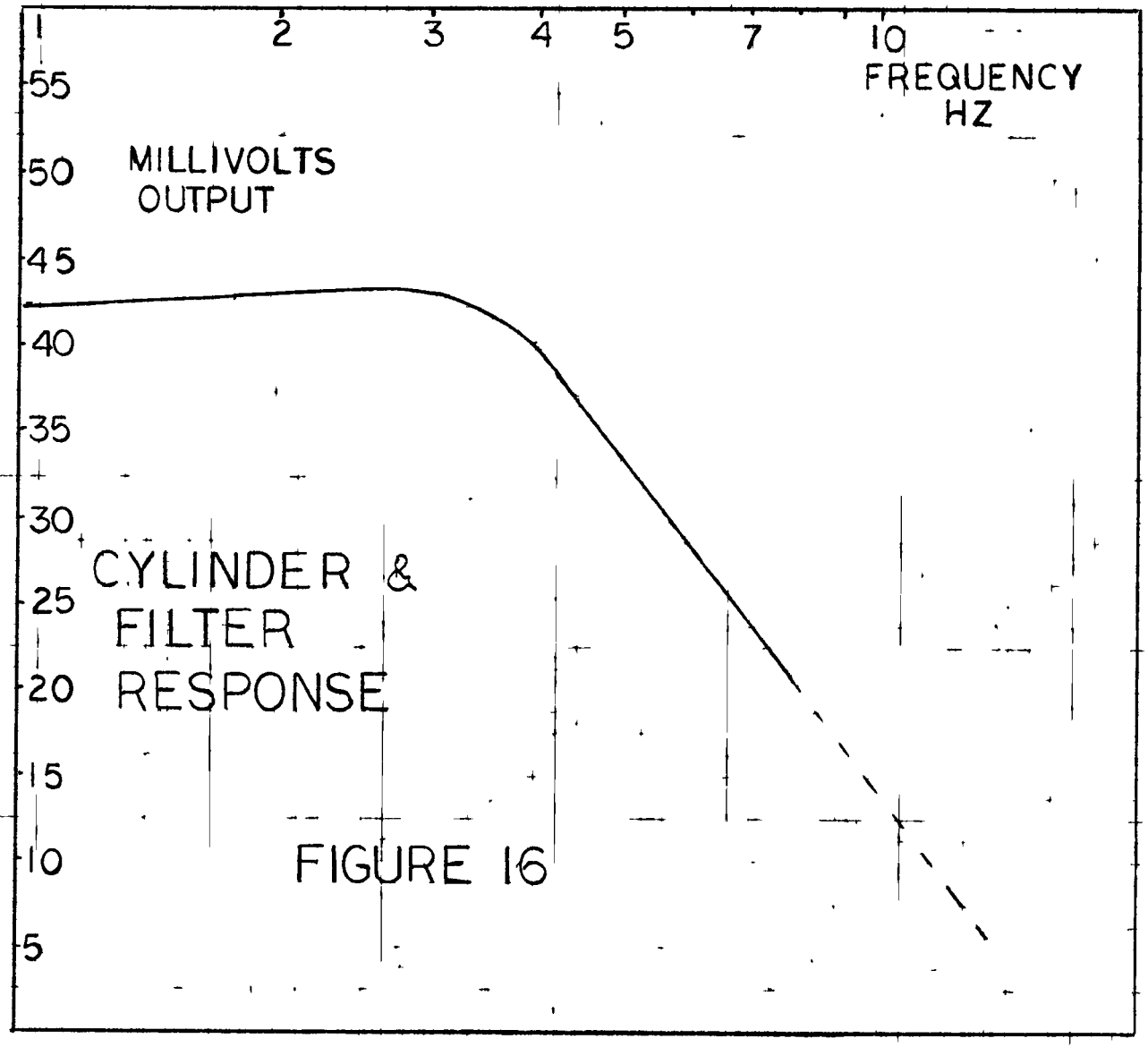
1
2
3
4
5
7
10
FREQUENCY
HZ
55
50
MILLIVOLTS
OUTPUT
45
40
35
30
25
20
15
10
5
CYLINDER &
FILTER
RESPONSE

FIGURE 16

Run Procedure

Amplitude to diameter ratios were altered by changing the stroke of the yoke with the adjustable slider block. A rule and scribe marks were used to double check the amplitude settings. Strokes of 2, 3, 4, 5, and 6 inches were used to yield amplitude to diameter ratios of 1, 1.5, 2.0, 2.5 and 3.0 and K values of 6.28, 9.42, 12.57, 15.71, and, 18.84.

When the stroke was set, runs at different speeds were made before resetting the machine stroke. A variable rheostat was used to drive the motor and the exact speed of the rig could not be accurately duplicated. Rough approximations were used to vary the speed between runs at a given stroke by 6 in/sec. Actual velocities were measured from the chart using the timing mark and chart speed. There was less than 2% variation between cycles so that there was very little slippage on the yoke drive even at the highest speeds run in the tests. However, yoke slippage is not the only cause of a period difference between cycles. More about this in the results discussion.

No less than 5 minutes elapsed between runs and several criteria were used to judge when the water had calmed enough to make a data run. First, the water itself would have to be visibly quiet. Second, the deflection of the

pen on the recorder at 2 millivolts per division gain had to be negligible with the rig stopped before the next run. The water could appear quiet on the surface but the cylinder could still move because of remaining vorticity and fluid motion.

In general this disturbance did not last more than 20 to 30 seconds after stopping the cylinder. In cases where the surface waves generated were negligible, the cylinder movement due to residual vorticity could still be present, even after the surface effects appeared to be gone. In all cases, after 5 minutes, no residual effects remained.

Before the run, the bridge amplifier was checked for bridge null and amplifier gain. The active filter was also checked. The rheostat was turned as quickly as possible to the desired setting and the system allowed to run until wave reflection from the sides of the tank reached the cylinder. Chart speed was selected at either 25 mm/sec or 125 mm/sec depending upon the oscillation period of the rig.

The wave gage was not used in every test. It was used on several runs at each amplitude-to-diameter ratio in order to measure the waves generated by the cylinder.

In order to be certain that the cylinder transducer beams were mounted perpendicular to the direction of travel,

marks were scribed using a square on top of the top fin. By locating the plane of maximum force with the cylinder in the horizontal plane, the position was found and the marks scribed into the aluminum fin. Then the cylinder was mounted to the yoke and locked into place with the scribe marks parallel to the yoke guidepiece.

Data Reduction

For each speed setting of the rig and each amplitude setting, as many cycles as practical were averaged to obtain a representative cycle. The same points in time on the curves were used to calculate the estimator of the mean millivolt value at that point. Along with the discrete point estimator, the standard error of the mean and interval estimators or confidence intervals were calculated. Tables and other data for the calculations are shown in Benedict [6]. Table I shows the results of such calculations for the maximum mean value of the millivolt readings for each data pass. This information is very useful as an indicator of the reliability of the overall results. The statistical analysis of the raw data coupled with the in-depth system analysis in the calibration section should aid understanding of the results to be discussed later.

An explanation of Table I is required. a/d is simply the amplitude-to-diameter ratio. The Keulegan-Carpenter number (K) is related to it by the following:

$$K = 2\pi\ a/d = \frac{U_m T}{d}\ , \tag{25}$$

where a is amplitude of oscillation, d is cylinder diameter, and U_m is the maximum velocity, N is the number of data sets for each point on the average curve, R is the range defined as the difference between the lowest and highest values at any given velocity or time. $\bar{x}$ at M.V.max is the mean value of the raw millivolt readings at the point where $\bar{x}$ is a maximum. $\bar{s}$ at M.V. maximum is the estimator for the standard error of the mean at the same point as $\bar{x}$ at M.V.max. Both relationships are functionally defined below,

$$\bar{x}\Big|_{M.V.max} = \frac{1}{N} \sum_{i=1}^{N} x_i\Big|_{M.V.max} \tag{26}$$

$$\bar{s}\Big|_{M.V.max} = \left[\frac{1}{N-1} \sum_{i=1}^{N} \left(x_i\Big|_{M.V.max} - \bar{x}\Big|_{M.V.max}\right)^2\right]^{\frac{1}{2}}\ , \tag{27}$$

where N is the number of data sets at the point, and $x_i|_{M.V.max}$ is the ith value at the curve's maximum.

The mean and standard error of the mean estimator are used to calculate the interval estimator or tolerance on the mean. This is referred to in Table I as the 95% confidence

TABLE I

a/d	U_m in/sec	N	$\bar{x}_{M.V.max}$ R at	$\bar{x}$ at M.V.max	$\bar{s}$ at M.V.max	95% Confidence Limit
1.0	14.34	6	5 at 11	11	1.76	± 1.85 M.V.
1.5	5.65	3	2 at 9	9	1.53	± 3.80 M.V.
1.5	12.88	6	4 at 30	30	2.80	± 2.94 M.V.
1.5	20.58	4	7 at 30	30	2.99	± 4.76 M.V.
2.0	5.03	6	2.5 at 6.5	6	1.08	± 1.13 M.V.
2.0	12.18	4	27 at 15	15	11.06	± 17.60 M.V.
2.0	19.51	4	85 at 58.75	38	45.04	± 71.66 M.V.
2.0	27.56	6	57 at 127	127	28.11	± 29.50 M.V.
2.5	11.06	5	14 at 45	45	5.29	± 6.57 M.V.
2.5	18.61	5	19 at 70	70	8.29	± 10.29 M.V.
2.5	26.17	4	23 at 122	112	23.5	± 29.17 M.V.
3.0	10.34	7	10 at 42	42	3.65	± 3.38 M.V.
3.0	17.13	7	82 at 92	92	26.8	± 24.79 M.V.
3.0	24.09	6	80 at 122	122	30.0	± 31.49 M.V.
3.0	31.77	3	20 at 175	175	5.0	± 12.42 M.V.
3.0	38.23	3	50 at 181	181	30.6	± 76.03 M.V.

limit. In short, this means that we are 95% certain that the true population mean with infinite samples lies within the range that the interval estimator defines. The interval estimator at 95% confidence is defined as

$$I.E./95\% = \frac{\pm\left(t_{N-1,.95}\right)\bar{s}}{\sqrt{N}}, \tag{28}$$

where $t_{N-1,.95}$ is the value of the Student t statistical distribution, $\bar{s}$ is the standard error of the mean estimator, and N is the number of data sets.

By analyzing the raw data in this manner, random errors can be accounted for and the final results better understood.

One other point is vital concerning data reduction. Phase shifting of the data trace occurs as the signal passes through the filter. This was an unavoidable situation but one which can be compensated for. The data trace was analyzed for its fundamental frequency and then the timing mark was shifted forward the appropriate amount. Figure 10 shows the phase shift curve over the range needed.

As far as the actual number of curves is concerned less than 3 points yield very poor accuracy statistically. The value of $t_{N-1,.95}$ when N = 2 is 12.706 but when N = 3, it is down to 4.303 and at N = 6, it is 2.447. To further put the analysis into perspective, an infinite number of data

points yields $t_{N-1,.95}$ of 1.96. The upshot is that little effort should be spared to get at least 3 curves but more than 3 does not increase data reliability significantly. This fact is discussed in Benedict [6].

CHAPTER 4

COMPUTATIONAL PROCEDURE

Force Calculation

A program was used to calculate the force from the raw millivolt readings taken from the curves off of the strip chart recorder. Equations (16) and (17) were used depending upon the sign of the millivolt reading for each point. The number of points used for each of the force curves shown in Figures 18, 19, 20, 21, 22, 23, and 24 was selected to give as smooth a curve as possible. The mean value or estimator of the mean millivolt value was used at each point in the cycle and a corresponding force value was calculated.

Velocity Calculation

The same program that calculated the force also calculated the velocity as well as lift coefficients. The velocity for the simple harmonic motion is given as

$$U = a\omega \cos(\omega t), \tag{29}$$

where a is amplitude, ω circular frequency, and t time. By replacing the circular frequency with harmonic frequency, f, we get

$$U = a\ 2\pi f \cos(2\pi f t). \tag{30}$$

The equation can be written as

$$U = 2\pi f a \cos\left(2\pi \frac{t}{T}\right), \tag{31}$$

where τ is period and t is time, and the units of radians can be changed to degrees and

$$U = 2\pi fa \cos\ (360\ \frac{t}{\tau}). \tag{32}$$

For easy reduction from the actual curves and using the number of millimeters distance from the point of maximum velocity, equation (35) is written as

$$U = 2\pi fa \cos\ (360\ \frac{d_i}{D}), \tag{33}$$

where d_i is the distance of the ith point on the curves and D is the total distance, both in millimeters. This is the relationship used in the calculating routine. For maximum velocity, the values of $\cos\ (360\ \frac{d_i}{D})$ is unity and

$$U_{max} = 2\pi fa \tag{34}$$

$C_{L\ max}(t)$ Calculation

Values of peak lift coefficient referenced to maximum velocity were calculated for the various points in the cycle,

$$C_{L\ max}(t) = \frac{F(t)}{0.5\ \rho dLU^2_{max}} \tag{35}$$

where F is the force at a particular time in the cycle, ρ is water density in the tank, d is cylinder diameter, L is test section length and U_{max} is the maximum velocity.

The same program that calculated force and velocity used these to calculate the lift coefficient at each time

in the cycle. The $C_{L\ max}(t)$ vs time curves are on the bottom of Figures 18, 19, 20, 21, 22, 23 and 24 for different values of amplitude to diameter ratio or K.

$\overline{C}_{L\ max}$ vs β Calculation

Plots of $\overline{C}_{L\ max}$ against β, the frequency parameter were also made. Figure 17 shows the results of the present work and Figure 17A shows the results of Sarpkaya [1]. In Figure 17, there are tolerances placed on each point. These were calculated by using the 95% confidence limit on the maximum force referred to maximum velocity. The equation for this is

$$\overline{C}_{L\ max} = \frac{F_{max}}{0.5\ \rho dL\ U^2_{max}} . \tag{36}$$

The parameter β is as defined in (3). Curves were fitted to their data using both a logarithmic and exponential function. This result should allow calculation of expected lift coefficient for given values of K and R. Coefficient of determination was also calculated for each of the curves representing the different values of K.

The values of $\overline{C}_{L\ max}$ are taken at the peak force not the semi-peak which is half the peak to peak. By looking at the $\overline{C}_{L\ max}$ vs time curves in Figures 18 through 24, the

peak and semi-peak are not necessarily equal. The peak and semi-peak are only equal for a perfect periodic function that is symmetric, i.e., a sine wave.

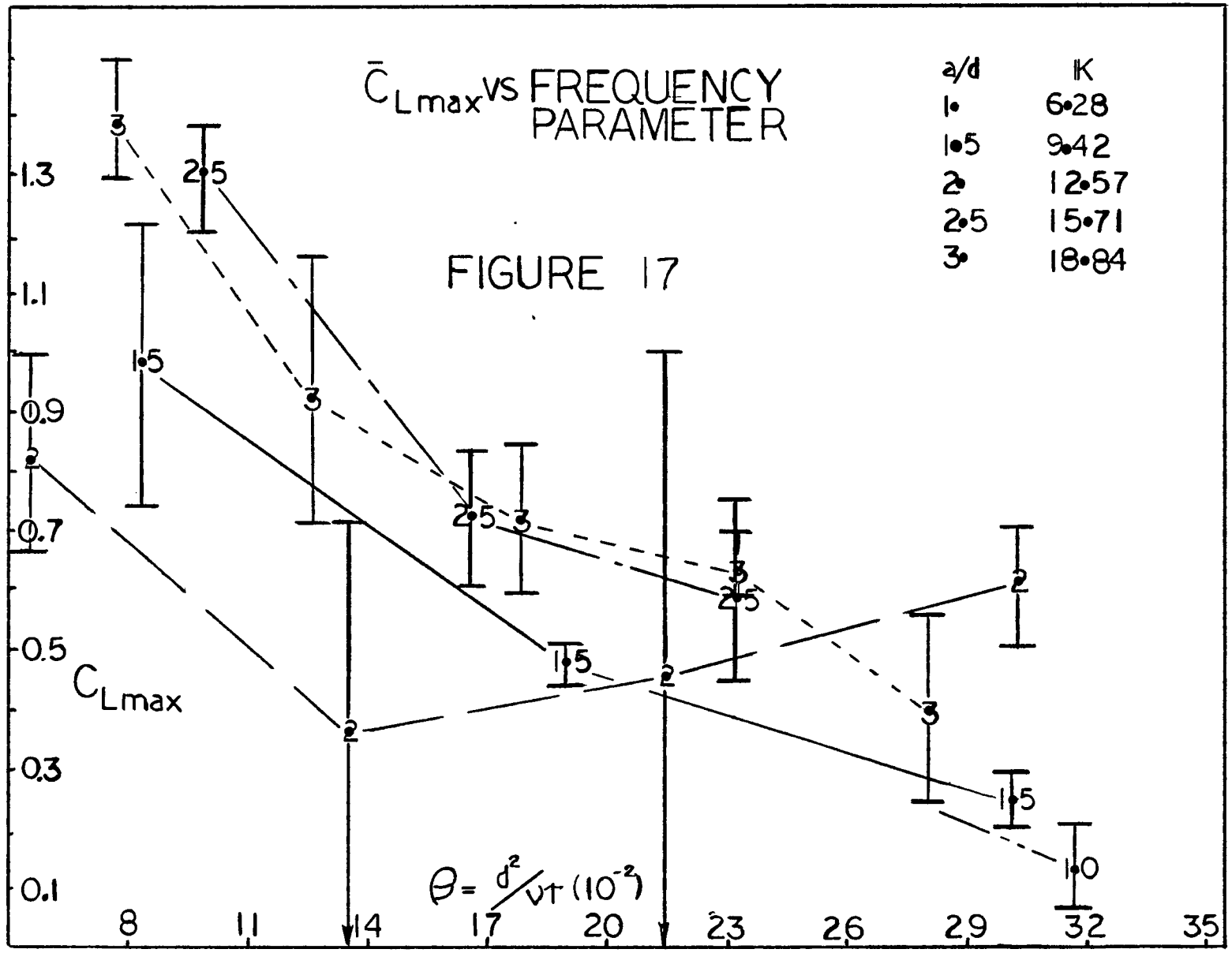
$\bar{C}_{Lmax}$ VS FREQUENCY PARAMETER
a/d
K
1•
6•28
1•5
9•42
2•
12•57
2•5
15•71
3•
18•84
C_{Lmax}
$\theta = d^2/\nu T\ (10^{-2})$
1.3
1.1
0.9
0.7
0.5
0.3
0.1
8
11
14
17
20
23
26
29
32
35

FIGURE 17

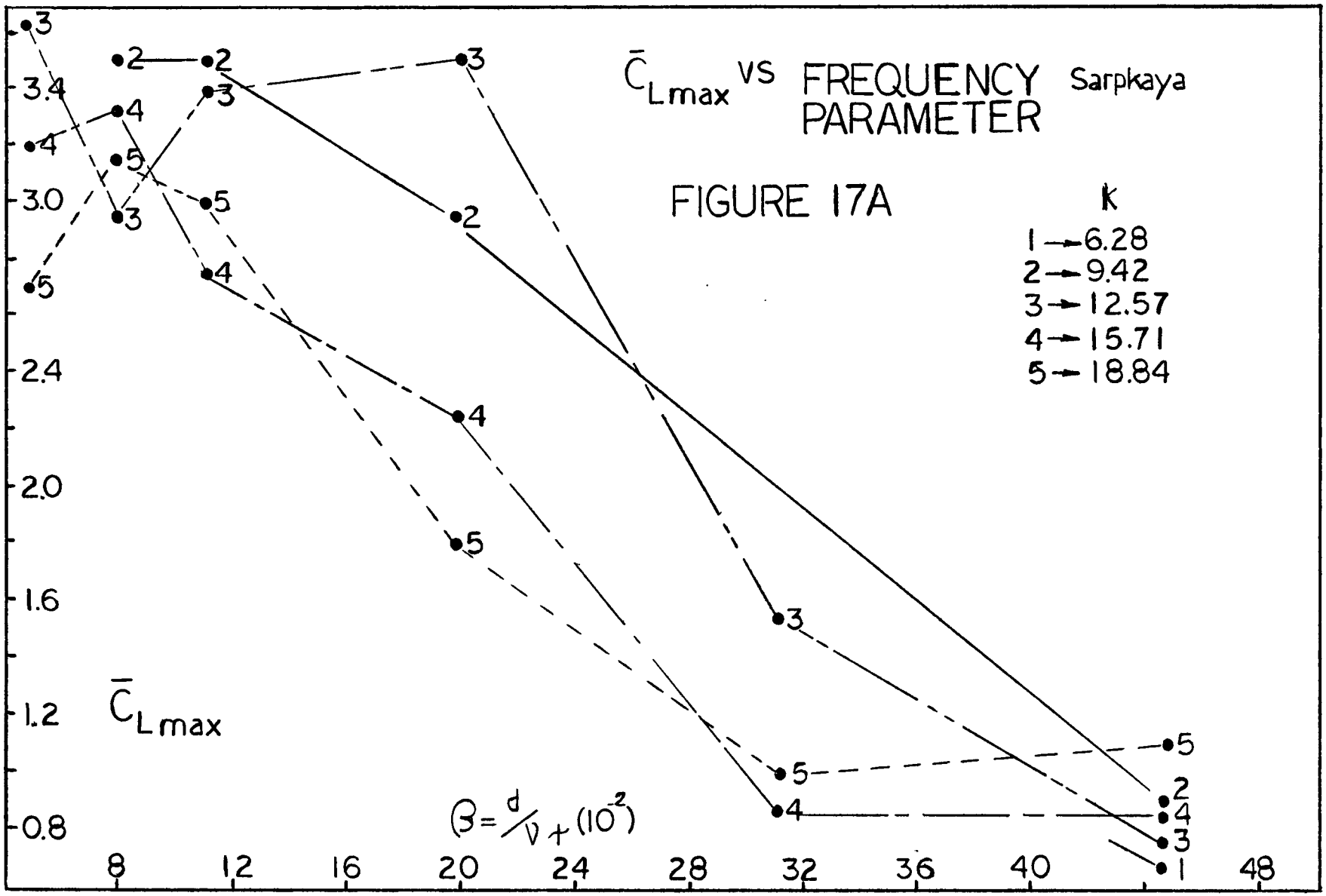
$\bar{C}_{L\,max}$ VS FREQUENCY PARAMETER
Sarpkaya
FIGURE 17A
k
1 → 6.28
2 → 9.42
3 → 12.57
4 → 15.71
5 → 18.84
$\bar{C}_{L\,max}$
$\beta = d/\nu + (10^{-2})$
3.4
3.0
2.4
2.0
1.6
1.2
0.8
8
12
16
20
24
28
32
36
40
48

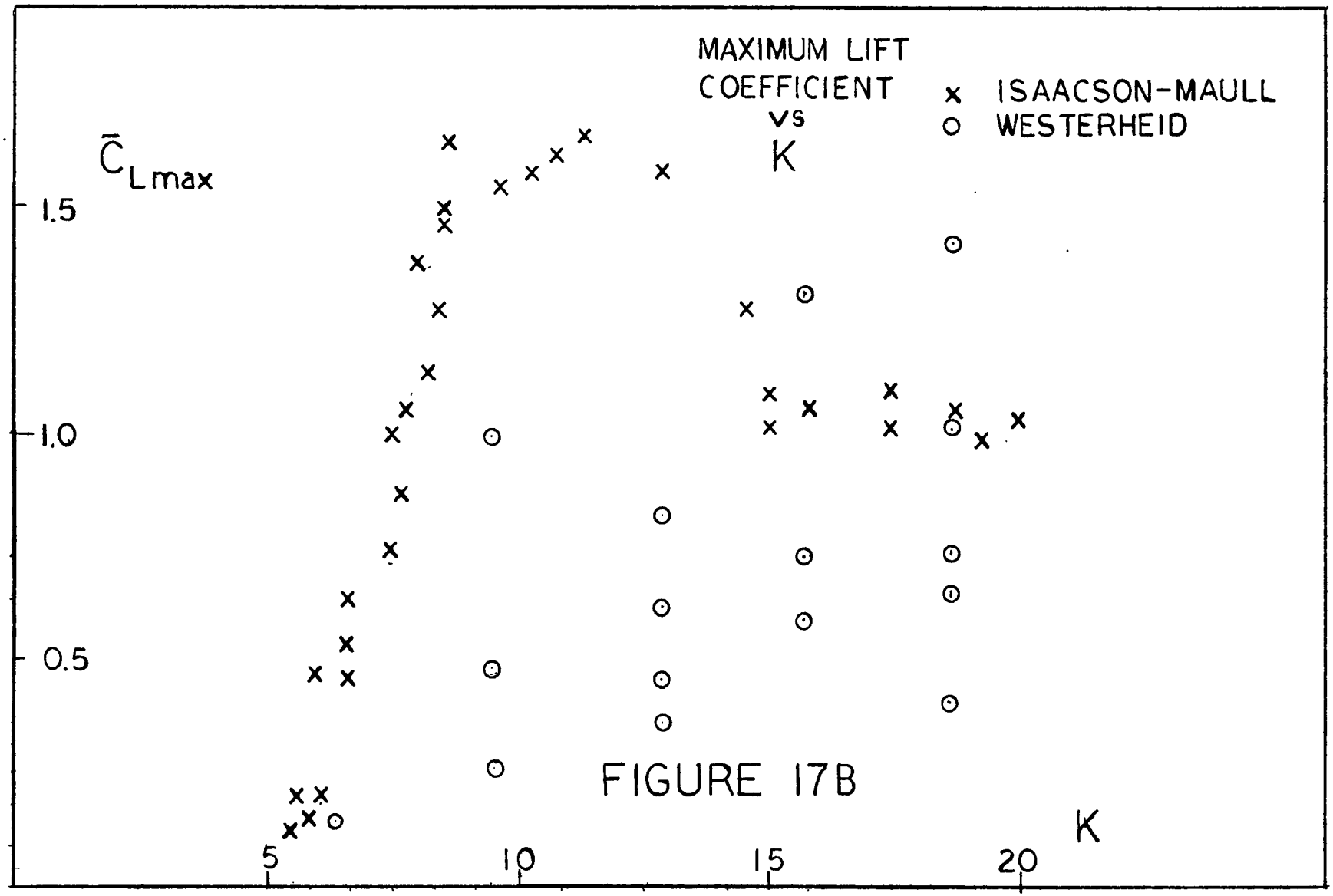
MAXIMUM LIFT
COEFFICIENT
vs
K
× ISAACSON-MAULL
○ WESTERHEID
$\bar{C}_{L\,max}$
1.5
1.0
0.5
5
10
15
20
K

FIGURE 17B

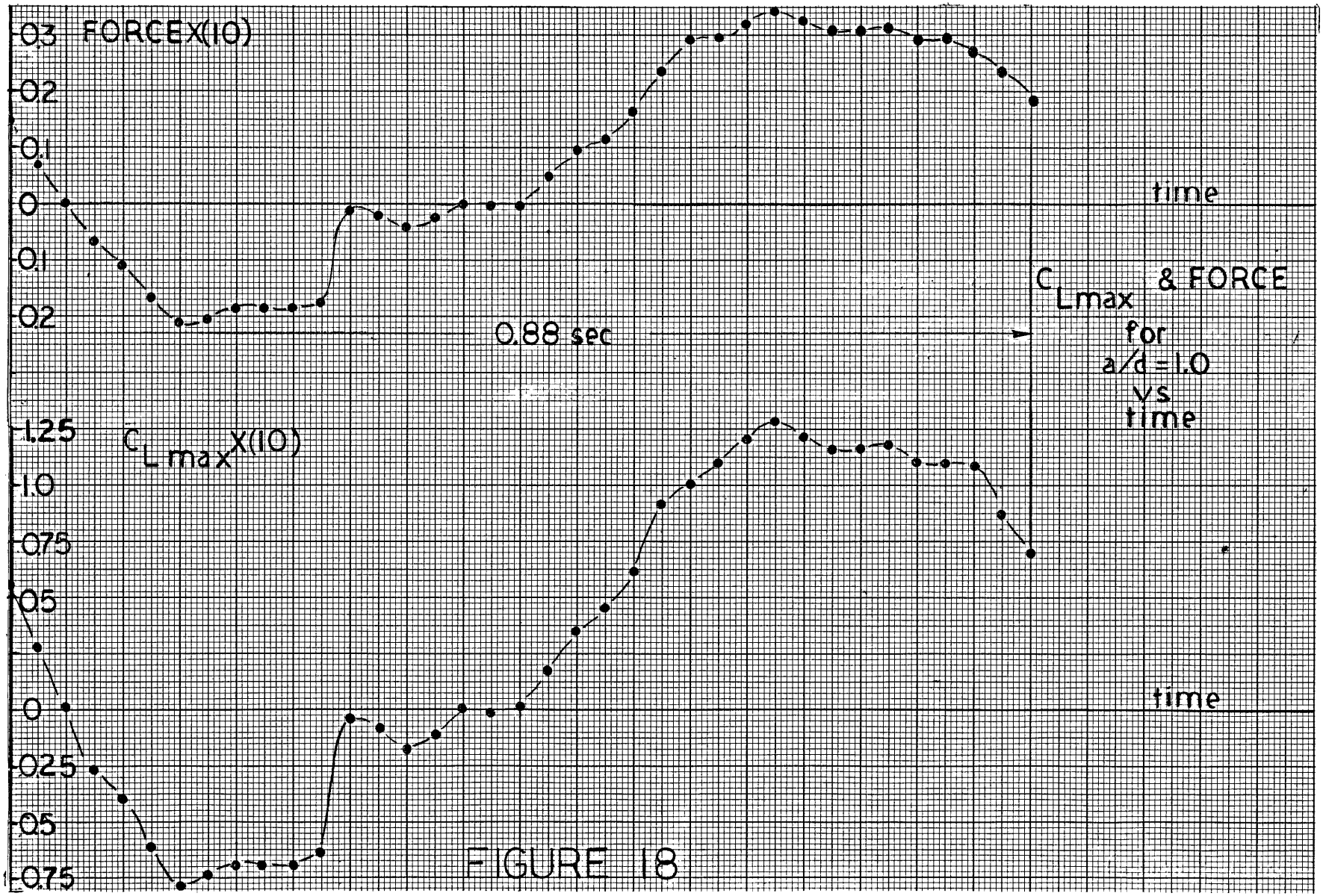
0.3 FORCEX(10)
0.2
0.1
0
0.1
0.2
time
C_{Lmax} & FORCE
for
a/d = 1.0
vs
time
0.88 sec
1.25
$C_{L\,max}X(10)$
1.0
0.75
0.5
0
0.25
0.5
0.75
time

FIGURE 18

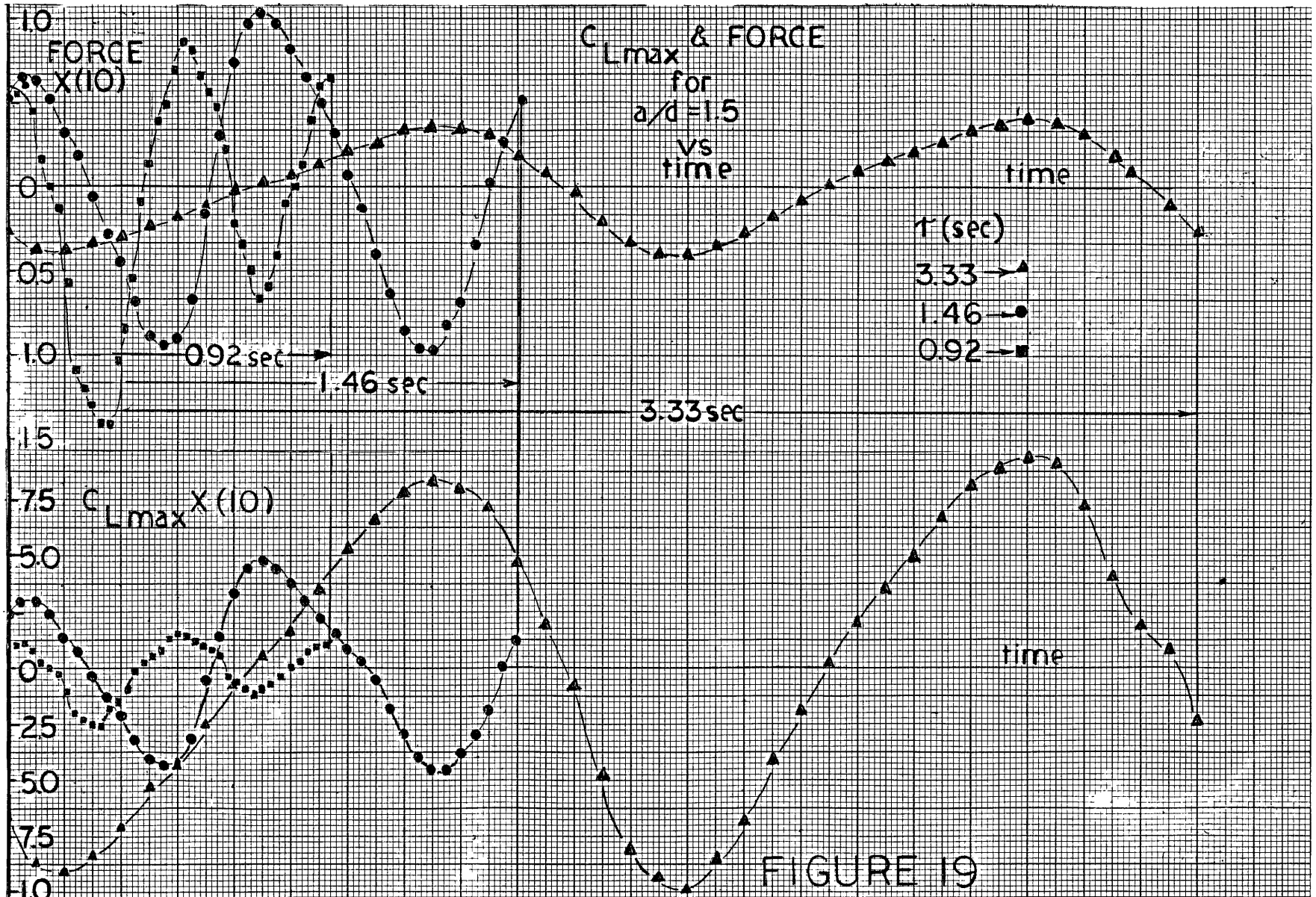
C Lmax & FORCE
for
a/d = 1.5
Vs
time
FORCE X(10)
C Lmax X (10)
time
T (sec)
3.33
1.46
0.92
0.92 sec
1.46 sec
3.33 sec
1.0
0
0.5
1.0
1.5
.75
5.0
0
.25
.50
.75
1.0

FIGURE 19

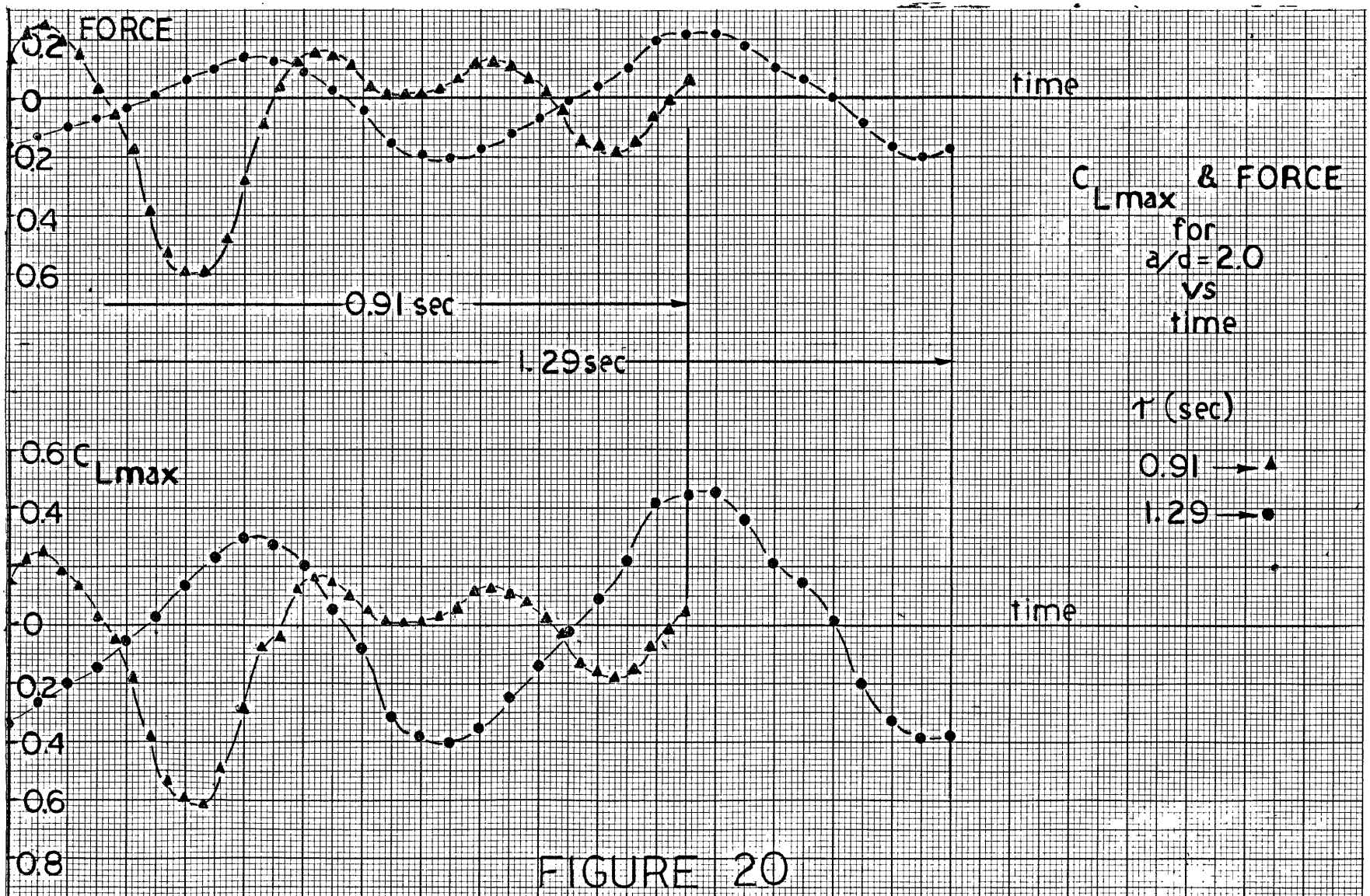
FORCE
0.2
0
0.2
0.4
0.6
time
0.91 sec
1.29 sec
C_{Lmax} & FORCE
for
a/d = 2.0
vs
time
τ (sec)
0.91
1.29
0.6 C_{Lmax}
0.4
0
0.2
0.4
0.6
0.8
time

FIGURE 20

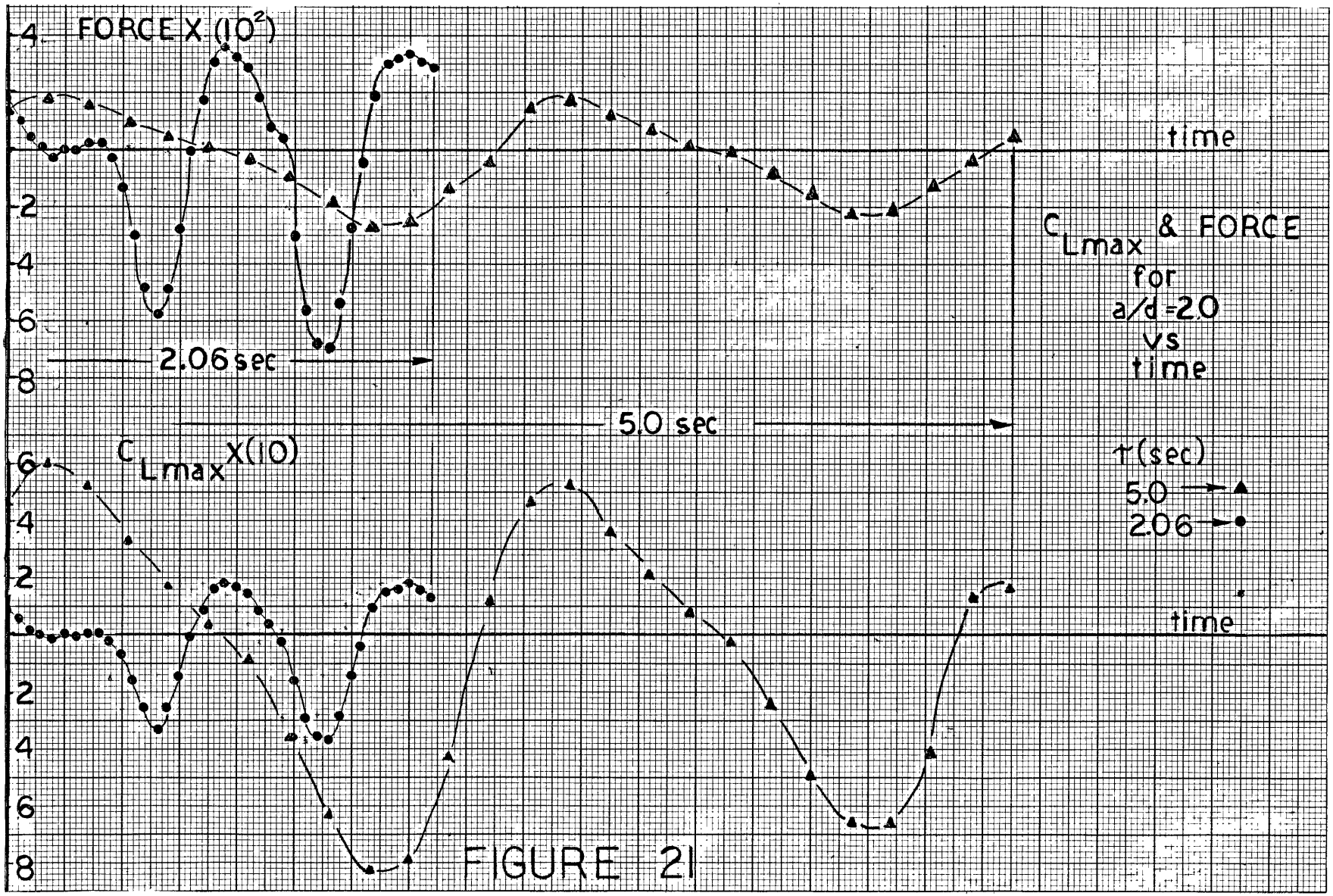
FORCE X (10²)
4
2
4
6
8
time
C Lmax & FORCE
for
a/d = 2.0
vs
time
2.06 sec
5.0 sec
C Lmax X(10)
6
4
2
2
4
6
8
τ (sec)
5.0
2.06
time

FIGURE 21

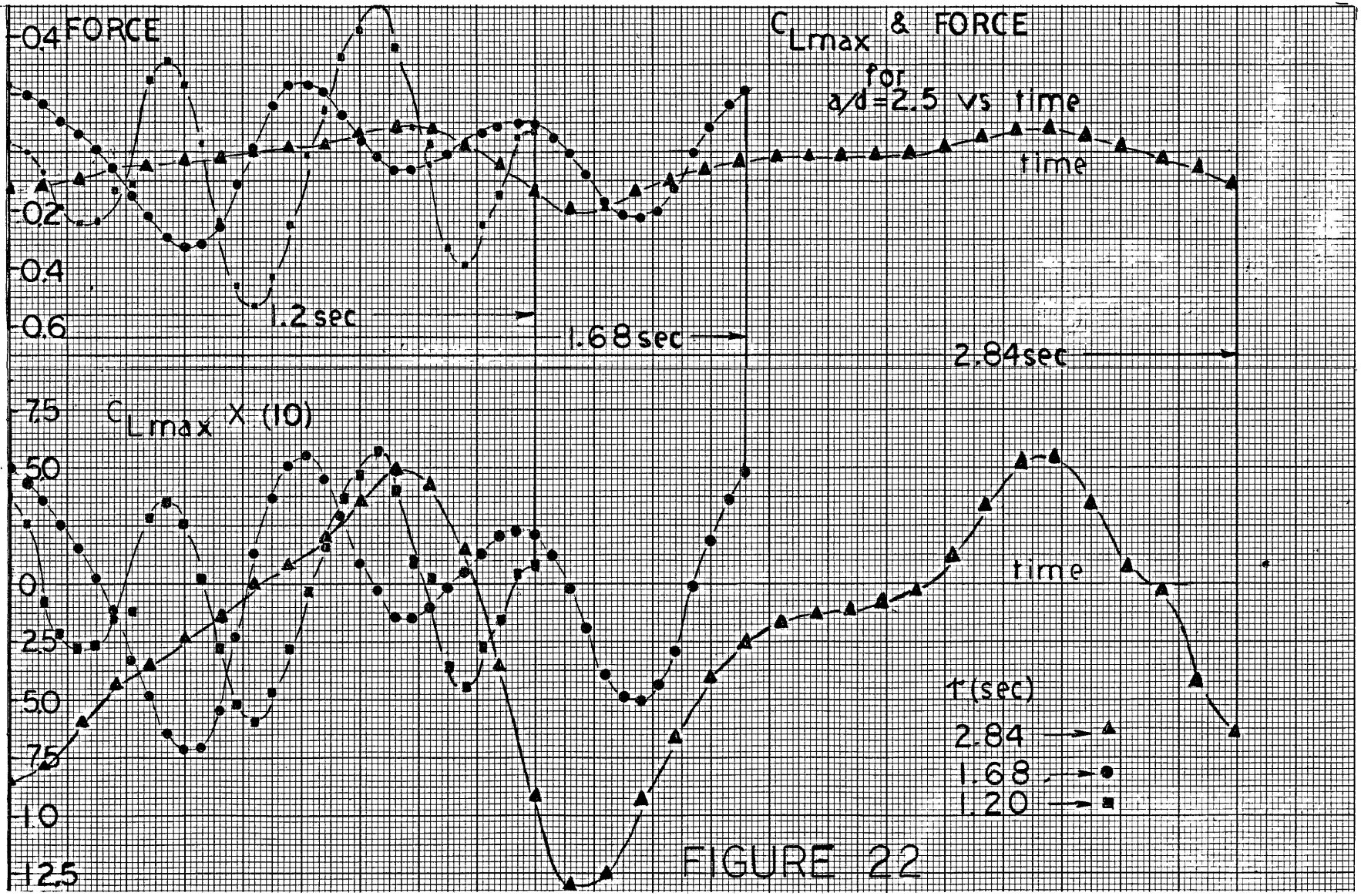
C_{Lmax} & FORCE
for
a/d=2.5 vs time
time
FORCE
.4
.2
0
.2
.4
.6
1.2 sec
1.68 sec
2.84sec
C_{Lmax} X (10)
.75
.50
0
.25
.50
.75
1.0
1.25
time
t (sec)
2.84
1.68
1.20

FIGURE 22

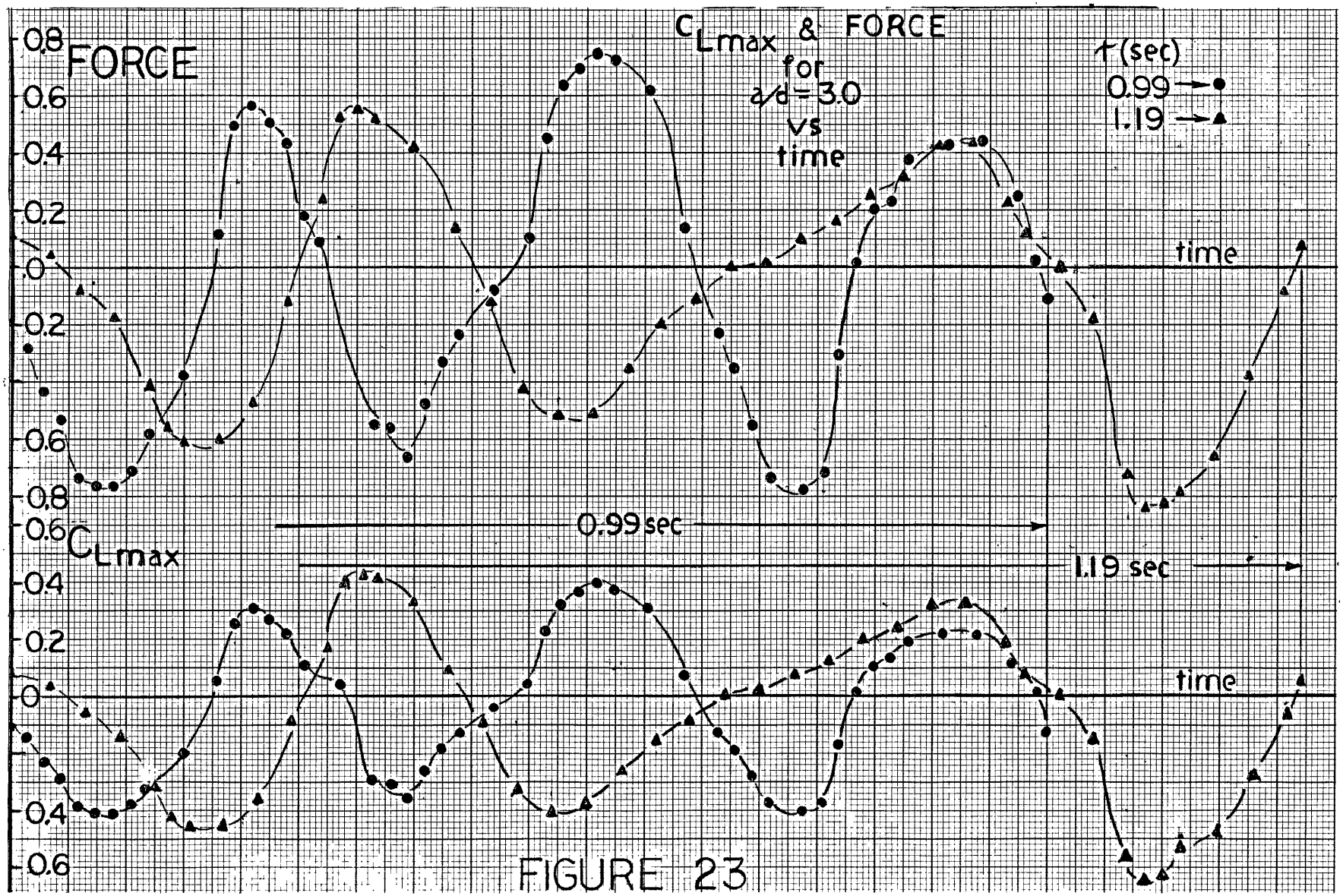
C_{Lmax} & FORCE
for
a/d = 3.0
vs
time
τ (sec)
0.99
1.19
FORCE
C_{Lmax}
0.8
0.6
0.4
0.2
0
0.2
0.6
0.8
0.6
0.4
0.2
0
0.4
0.6
time
time
0.99 sec
1.19 sec

FIGURE 23

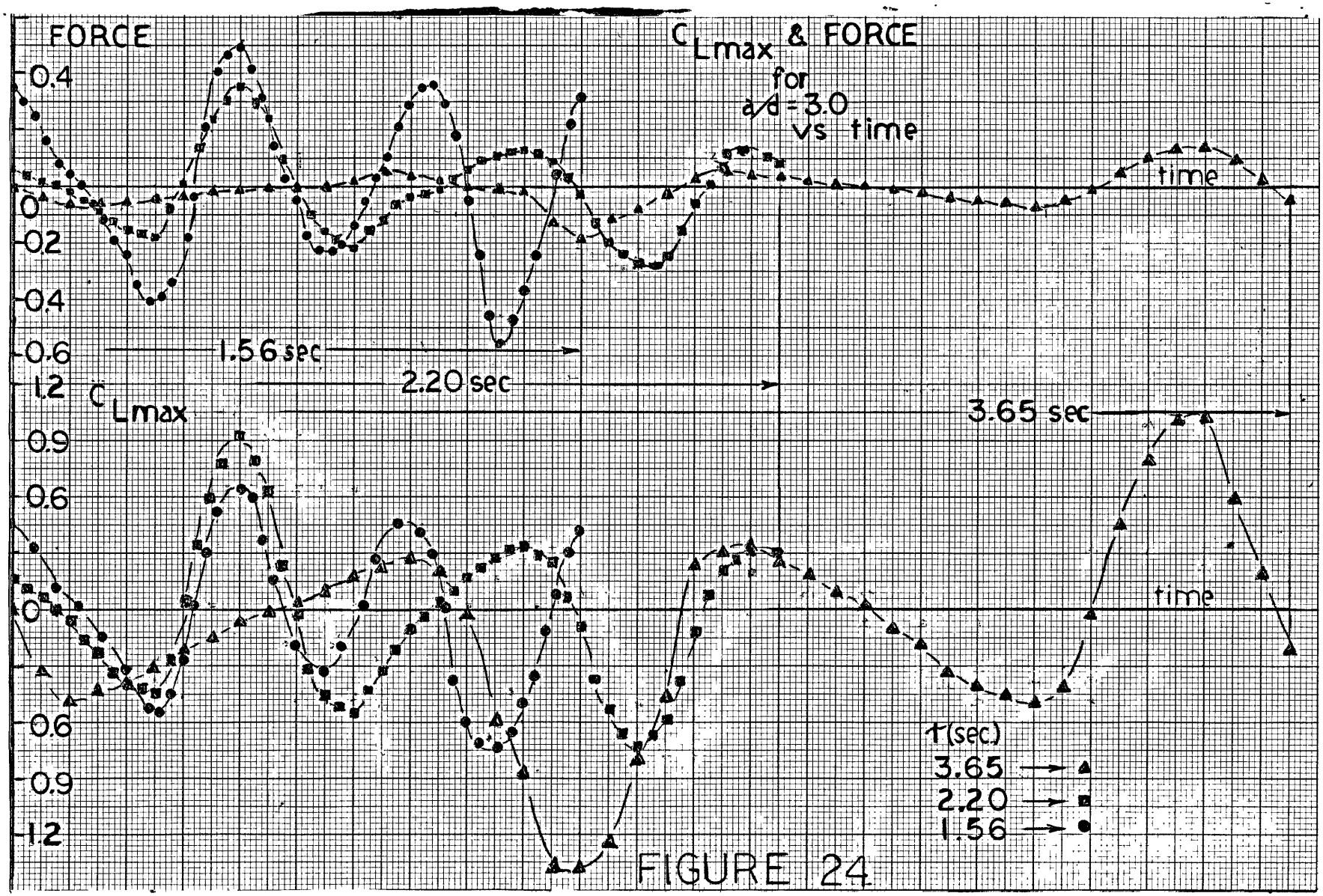
FORCE
C_{Lmax} & FORCE
for
a/d = 3.0
vs time
0.4
0
0.2
0.4
0.6
1.2
C_{Lmax}
0.9
0.6
0
0.6
0.9
1.2
1.56 sec
2.20 sec
3.65 sec
time
time
τ(sec.)
3.65
2.20
1.56

FIGURE 24

CHAPTER 5

RESULTS AND DISCUSSION

In general, Figures 18, 19, 20, 21, 22, 23, and 24 are average curves. Table I shows how many curves or cycles were used to obtain the average curves shown. Thus $\overline{C}_{L\ max}$ is the maximum mean value and not the highest value obtained during the tests. Figures 17 and 17B are plots of these maximum mean values of lift coefficient against β and K. All of the curves start at the point of maximum velocity and finish at maximum velocity. A point of maximum velocity also occurs within each curve at $\tau/2$.

Figure 18 shows results for a/d of 1.0. This yields K of 6.28. The period for this curve was 0.88 seconds. During this period, there appears to be only one cycle of force fluctuation. The actual data traces verified $\overline{C}_{L\ max}$ peaks at 0.13. Longer periods, runs with lower velocities and accelerations, yielded no detectable flucutations in force. These curves are averages of 6 cycles. Note that the average curve "hunts" before it crosses the time axis. What is happening is that the physical phenomenon of vortex shedding <u>is not</u> periodic over the time periods involved in this study. There are narrow band random fluctuations. Both the period or frequency and ampltidue vary from one cycle

to the next. This is true at all values of K and β studied in this research. In some of the average curves, this phenomenon does not have enough effect to show up. The total system is not determinable as to mass, spring constant and damping. The cylinder subsystem is, but its interaction with the water is not.

At this value of K (6.28) we are at the lower end of the range of K where lift occurs. At the lower frequencies and periods for K = 6.28, less energy is input to the "system" and there may not be enough disturbance to allow the vortices to become asymmetric. Figure 1 illustrates this situation. At shorter periods, much more energy is put into the system and more vorticity must be dissipated. The value of R and β are both higher for shorter periods. The parameter β has more complete definition of the phenomenon than K or R alone. As Wiegil [9] states, the total period or distance travelled is more important than the maximum velocity or R_{max}. It takes time for vorticies to develop and shed. The phenomenon itself of vortex shedding is transient.

Figure 19 shows results for a/d of 1.5 or K of 9.42 and periods of 3.33, 1.46 and 0.92. For this value of K, one vortex is shed per half cycle or two per full cycle. The curves show this type of shedding as does Figure 1. Another factor is the asymmetry of the curves in Figure 19. This

happens because when a vortex is shed, it causes an induced velocity which affects the velocity of the free stream or cylinder velocity when the cylinder returns on the last half of the cycle. This addition of velocity can be explained because the vortex is rotating and effectively increases the relative velocity between cylinder and water and forces the stronger vortex to remain on the same side of the cylinder from cycle to cycle. Figure 1 shows this for K = 8. The same wave shape exists in all three curves. Heinzer [3] found that for a given value of a/d or K the nature of shedding did not change. In the present research, period or frequency made no significant difference in the wave shape of the average curves. The curves in Figure 19 show that the force and lift coefficient curves are different for different periods. This illustrates the importance of the frequency parameter, β. Narrow band random fluctuations do not have a pronounced effect on these average curves. Maximum lift coefficients, $\overline{C}_{L\ max}$, were 0.98, 0.48, and 0.25 for periods of 3.33, 1.46, and 0.92 respectively. The shorter periods had higher peak velocities but did not have enough time at the higher velocities and R to develop enough force to give higher values of $\overline{C}_{L\ max}$ than lower periods.

Figures 20 and 21 show results for a/d of 2.0 or K of 12.57 and periods of 5.0, 2.06, 1.29 and 0.91 seconds. The

period of 5.0 seconds is the highest period at which significant fluctuations were measured in force. This does not say it is the highest period, lowest frequency, or lowest β value at which fluctuations can occur. Using a variable rheostat to modulate motor speed did not give the freedom to preset the harmonic frequency exactly; only roughly.

In reality, lift may still be occurring at lower β values but the measurement system cannot detect it reliably. All curves have the characteristics of one vortex per half cycle. According to Sarpkaya [1] and Isaacson and Maull [4], a K value of around 15 is needed to obtain two vortices per half cycle. On the curves for 0.91 and 2.06 seconds period, we again notice the effects of random fluctuations. Two additional inflection points occur in the curves at these periods. This would appear to add another cycle during the oscillation period to each of these average curves. In reality, this is not the case. It is not physically happening that the cylinder is oscillating as the curve indicates. While the average curves for periods of 0.91 and 2.06 seconds show an apparent qualitative difference the curves for 2.06 and 1.29 have the most variation in peak amplitude for $C_{L\ max}$ and force. This is shown both in Table I and Figure 17 for a/d of 2.0. All of this serves to indicate the

necessity of a statistical approach to the problem. Maximum peak lift coefficients, $\overline{C}_{L\ max}$, were 0.82, 0.36, 0.45, and 0.61 for periods of 5.00, 2.06, 1.29 and 0.91 seconds respectively. The trend toward decreasing $\overline{C}_{L\ max}$ with increasing β is reversed here. There is no apparent physical explanation for this at present.

Figure 22 shows results for a/d of 2.5 or K of 15.71 and periods of 2.84, 1.68, and 1.2 seconds. At K = 15, the expected behavior is a transition to two vortices shed per half cycle. The curves for periods of 1.2 and 1.68 seconds show this to be the case. The curve for the 2.84 second period does not. Since the force is not very high in comparison to the other two curves; it is tempting to say that random fluctuations "cancelled" a cycle. Examination of the actual data trace shows this is not the case. The value of β may be too low for development of the second vortex to the size needed for shedding. There are regions of fractional shedding. These are regions with any given value of R and β for a set value of K where the last vortex in a half cycle does not shed. The last vortex does not grow large enough to be shed. Five curves were averaged and Table I clearly shows a very tight value of I.E. In other words what may have happened was that the system changed from two vortices per half cycle after only 2

cycles from start to one shed and perhaps one almost shed in each half cycle. Perhaps there is not enough energy available after shedding the first vortex for the second one to develop to shedding in the distance that remains until reversal of the cycle. Since Reynolds number is actually time variant, there should be enough time to develop and shed the second vortex even though R is not as high as in curves of 1.2 and 1.68 seconds. However, there is no force reversal on the actual data traces, merely a tendency toward zero slope in the curves after the "first" vortex in the half cycle is shed.

Maximum lift coefficients, $\overline{C}_{L\ max}$, of 1.3, 0.72, and 0.59 were obtained for periods of 2.84, 1.68, and 1.2 seconds. Again, the trend is to increasing lift coefficient for decreasing frequency parameter, β. Also the trend has been established that we have an increasing $\overline{C}_{L\ max}$ for increasing K at comparable values of β. Little effect in the nature of the curves can be attributed to random fluctuation.

Figures 23 and 24 show results for a/d values of 3.0 or K of 18.84 and periods of 3.65, 2.2, 1.56, 1.19, and 0.99 seconds. All of these traces show similar behavior. There is more effect from random fluctuation in the two curves of highest frequency. Amplitude variations are greatest at 0.99 and 2.20 seconds period but there seems to be less

random phase changes as period increases. The regime of two vortices shed per half cycle exists here and all curves show 6 half cycles or force peaks. Remember, a vortex does not have to be shed to obtain lift, so 2 vortices shed per half cycle can mean 3 force peaks per half cycle. Maximum lift coefficients, $\overline{C}_{L\ max}$, were 1.39, 0.94, 0.73, 0.64, and 0.40 for periods of 3.65, 2.2, 1.56, 1.19, and 0.99 seconds respectively.

In summarizing the results of these curves, it is most important to discuss frequency of the lift force. As Sarpkaya [1] points out all vortices are not necessarily shed. This fact along with previously discussed narrow band fluctuation forces one to recognize that again K does not tell the complete story. Figure 25 shows that both lower and higher values of f_L/f_o, the ratio of lift frequency to water oscillation frequency, can be obtained at higher and lower values of K. Notice that we had a f_L/f_o ratio of 1.0 at a/d = 1.0 and K = 6.28. There is no vortex shed but asymmetry does develop. Also at a/d = 2.5 (τ = 2.84 seconds period and K = 15.7), we obtained a value of 2 for the nearest integer lift frequency. This would suggest only one vortex shed per half cycle on this particular run. This is most probably what happened. In general as Figure 25 shows the lift frequency is highly predictable based on K. Plotted

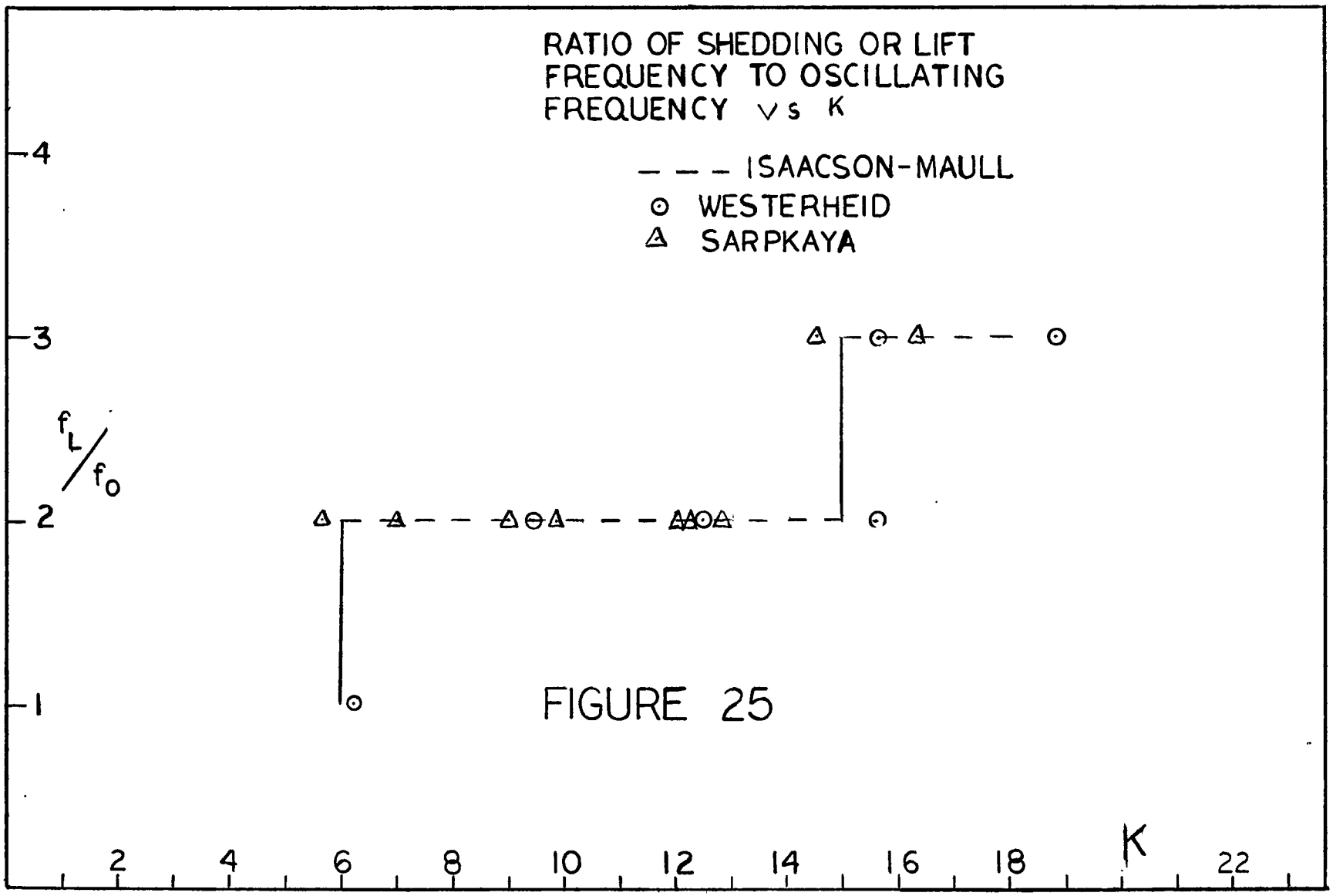
RATIO OF SHEDDING OR LIFT FREQUENCY TO OSCILLATING FREQUENCY vs K
ISAACSON-MAULL
WESTERHEID
SARPKAYA
4
3
2
1
f_L/f_0
2
4
6
8
10
12
14
16
18
22
K

FIGURE 25

on Figure 25 are some of the points Sarpkaya computed and the values for the present work. The dotted line is the expected behavior as described by Isaacson and Maull [4] and found by Chakrabarti [7] with just a few exceptions. The exceptions were as plotted on Figure 25 wherein a few values of f_o/f_L were one cycle lower than one would intuitively expect. These exceptions are for lower values of R and β. Figure 54 in [1] shows this exception also.

Also, from Figures 17, 17A, and 17B we can see the upshot of the force measurements. Figure 17 shows the mean values of lift coefficient at the maximum peaks plotted against the frequency parameter, β. Using the confidence intervals for the mean peak forces from Table I, the values of the tolerance on the lift coefficients were calculated using the following:

$$\text{I.E.}\left|_{\overline{C}_{L\ max}}\right. = \frac{\text{I.E.}\left|_{\overline{F}_{max}}\right.}{0.5\ \rho dL\ U^2_{max}} \tag{37}$$

where $\text{I.E.}\left|_{\overline{F}_{max}}\right.$ is calculated from the values of the 95% confidence limits on $\overline{X}$ at M.V._{max}, and ρ, d, L, and U^2_{max} are as defined for previous expressions. It can be argued that intervals in ρ, d, L, and U_{max} should also be calculated. As a practical matter, there is no randomness in these values, only errors in precision of their measurement.

Figure 17 and 17A show a strong trend with β for a decrease in $\overline{C}_{L\ max}$. The difference between the two figures is that $\overline{C}_{L\ max}$ in Figure 17A is not an average value. $\overline{C}_{L\ max}$ in Figure 17A is the maximum value found. This is not apparent from reading the text of Sarpkaya [1] but in looking at the tabulated data where $C_{L\ R.M.S.}$ is printed with $\overline{C}_{L\ max}$ it seems the case. Figure 17B shows a comparison of Isaacson and Maull [4] and the present work. All of these figures were plotted on rectilinear scales. This was because, as Table II shows, the least squares curve fits in some cases showed higher coefficients of determinations for an exponential curve than for a logarithmic curve.

The data in Figure 17 was fitted to both logarithmic and exponential curves given respectively in the form

$$\overline{C}_{L\ max} = A + B\ell n\,\beta \tag{38}$$

and

$$\overline{C}_{L\ max} = C\beta^{D}; \tag{39}$$

where A, B, C, and D are constants to be determined. Then the equations were rearranged so that maximum peak force could be calculated. These relations are of the form:

$$\overline{F}_{max} = M(A + B\ell n\,\beta) \tag{40}$$

and

$$\overline{F}_{max} = MC\beta^{D} \tag{41}$$

TABLE II

d	K	LOGARITHMIC	r^2	EXPONENTIAL	r^2
1.0	6.28	INSUFFICIENT DATA			
1.5	9.42	$\bar{F}_{max}=M[4.82-0.57\ell n\,\beta]$	1.0	$\bar{F}_{max}=M\ 1110\beta^{1.04}$	0.98
2.0	12.57	$\bar{F}_{max}=M[1.65-0.15\ell n\,\beta]$	0.30	$\bar{F}_{max}=M\ 2.62\beta^{0.22}$	0.20
2.5	15.7	$\bar{F}_{max}=M[7.10-0.84\ell n\,\beta]$	0.95	$\bar{F}_{max}=M\ 788\beta^{0.93}$	0.98
3.0	18.84	$\bar{F}_{max}=M[6.06-0.71\ell n\,\beta]$	0.97	$\bar{F}_{max}=M\ 438\beta^{0.86}$	0.94
ALL		$\bar{F}_{max}=M[3.99-0.45\ell n\,\beta]$	0.54	$\bar{F}_{max}=M\ 229.2\beta^{0.81}$	0.52

where $M = 0.5\ \rho dLU^2_{max}$

where $M = 0.5\ \rho dLU^2_{max}$, the denominator of the dimensionless lift coefficient. With the force equation from Table II and calculation of the forcing frequency from Figure 25, one should be able to predict fatigue effects on piles, pipes and offshore platform legs as well as have some knowledge of the nature of a dynamic forcing function due to alternating lift on these bodies.

In Table II the logarithmic curve fits best except at K of 15.7. Neither curve fits well at K of 12.57 as indicated by the low values of the coefficient of determination r^2.

The results from the wave gage indicated that the maximum surface wave generated by the rig was 0.75 inch peak to peak at a/d of 3.0 or K of 18.8 and β of 1805. The wave length was not monitored.

CHAPTER 6

UNCERTAINTY ANALYSIS

The data used for the calculation of the results could have a definite bearing on the outcome. Due to errors of precision in the measurements taken on some of these data, an uncertainty analysis is needed. Equation (39) represents the relationship used to obtain the maximum lift coefficient for any value of K and β. By using the methods set forth by Kline and McClintock [10], the uncertainty in the maximum lift coefficient can be calculated. These uncertainty intervals are not the same as the interval estimator, I.E., defined in (40). The interval estimator took the narrow band random fluctuations in force into account. The uncertainty interval accounts for precisional errors in measuring cylinder dimensions, cylinder velocity, and water density.

The uncertainty interval is defined as

$$U.I._{\bar{C}_{L\ max}} = \left[\left(\frac{\partial \bar{C}_{L\ max}}{\partial \rho}\Delta\rho\right)^2 + \left(\frac{\partial \bar{C}_{L\ max}}{\partial d}\Delta d\right)^2 + \left(\frac{\partial \bar{C}_{L\ max}}{\partial L}\Delta L\right)^2 + \left(\frac{\partial \bar{C}_{L\ max}}{\partial U_{max}}\Delta U_{max}\right)^2 + \left(\frac{\partial \bar{C}_{L\ max}}{\partial \bar{F}_{max}}\Delta \bar{F}_{max}\right)^2\right]^{\frac{1}{2}} \tag{42}$$

where $\bar{C}_{L\ max}$ is defined in (40). Computing the partial derivatives gives

$$U.I.\Big|_{\overline{C}_{L\ max}} = \left[\left(\frac{-\overline{F}_{max}}{0.5\ \rho^2 dLU^2_{max}}\Delta\rho\right)^2 + \left(\frac{-\overline{F}_{max}}{0.5\ \rho d^2 LU^2_{max}}\Delta d\right)^2 + \left(\frac{-\overline{F}_{max}}{0.5\ \rho dL^2U^2_{max}}\Delta L\right)^2 + \left(\frac{-2\overline{F}_{max}}{0.5\ \rho dL^2U^3_{max}}\Delta U_{max}\right)^2 + \left(\frac{\Delta\overline{F}_{max}}{0.5\ \rho dLU^2_{max}}\right)^2\right]^{\frac{1}{2}}. \qquad (43)$$

The following tolerances were used as estimated.

$$\Delta\rho = 0.001 \text{ slugs/ft}^3$$
$$\Delta d = 0.01 \text{ inch}$$
$$\Delta L = 0.01 \text{ inch}$$
$$\Delta U_{max} = 0.006\ U_{max}, \text{ inch/second}$$
$$\Delta\overline{F}_{max} = 0.01 \text{ lb}_f$$

The tolerance in the force measurement is due mostly to the 2 millivolt noise. Initially the 60 Hz line noise was 80 millivolts but the filter cut it down to 2 millivolts. The tolerance in ρ was obtained by allowing ρ to be assumed as low as 62.3 lb/ft^3. The tolerances on d and L were measured and specified on assembly drawing for the cylinder. The tolerance in U_{max} is obtained by observing the change in distance of the timing marks on the strip chart due to drive belt slippage on the yoke. Using the above values for tolerances and

$$\rho = 1.94 \text{ slugs/ft}^3$$
$$d = 2.00 \text{ inches}$$
$$L = 13.37 \text{ inches},$$

and the appropriate values of $\overline{F}_{max}$ and $\overline{U}_{max}$ at various values of K; Table IV is developed from the following equation

$$U.I._{|\overline{C}_{L\ max}} = \frac{1}{U^2_{max}}\left[0.00116\ \overline{F}^2_{max} + 0.0003\right]^{\frac{1}{2}}. \qquad (44)$$

Since errors or tolerances in the actual values were small, the uncertainties are all very small. The largest uncertainty was in the force itself with the 2 millivolt noise. In fact, with periods of oscillation large enough, force flucutations could be imperceptable even though substantial lift coefficients would have resulted due to low velocities.

TABLE III

a/d	K	$\overline{F}_{max}$ lb	U_{max} w/sec	$\overline{C}_{L\ max}$	U.I. $\lvert\overline{C}_{L\ max}$
1.0	6.28	0.035	14.34	0.13	.00003
1.5	9.42	0.041	5.65	0.98	.00001
1.5	9.42	0.104	12.88	0.48	.00003
1.5	0.42	0.14	20.58	0.25	.00002
2.0	12.57	0.03	5.03	0.82	.0002
2.0	12.57	0.07	12.18	0.36	.00004
2.0	12.57	0.22	19.51	0.45	.00002
2.0	12.57	0.61	27.56	0.61	.00003
2.5	15.71	0.21	11.06	1.30	.00007
2.5	15.71	0.325	18.61	0.72	.00004
2.5	15.71	0.53	26.17	0.59	.00003
3.0	18.84	0.19	10.34	1.39	.00008
3.0	18.84	0.36	17.13	0.94	.000046
3.0	18.84	0.55	24.09	0.73	.00003
3.0	18.84	0.84	31.77	0.64	.00003
3.0	18.84	0.77	38.23	0.40	.00002

CHAPTER 7

CONCLUSIONS

As a result of the work presented here, several conclusions were reached. They are explained below.

1.) The shedding frequency is strongly dependent on K. It is almost independent of β. As Wiegel [9] states, it is the distance moved by the pile that is most important. The distance the fluid moves along the boundary determines the extent of backflow, separation, and vortex formation. This is true provided R is sufficiently large. In the case of water with the values of a/d used herein, there is always sufficient R to get vortex formation but a/d may not be large enough to get separation at all β values.

2.) The actual forces measured were in good agreement with those obtained by two separate methods. Sarpkaya [1] held the cylinder stationery and used a U-tube of elaborate design and construction and Isaacson and Maull [4] made waves past a stationary pile. In this work, a cylinder was moved with simple harmonic motion in a large wave tank otherwise at rest. As Figure 17 shows, maximum peak lift coefficient is strongly dependent on β the ratios of R to K. Sarpkaya's [1] data in Figure 17A bears this out.

3.) There are narrow band random fluctuations that are the nature of the phenomenon. The use of frequency domain

spectrum analysis does not sufficiently uncover this. In the present work, time domain plots of system response on an average basis showed these effects in Figures 18, 20, and 21 where they were most pronounced. These random fluctuations represent both variation in phase and amplitude from cycle to cycle. In the case of this work the amplitude variation was most significant.

4.) Maximum peak force can be modeled with either logarithmic or exponential curves with excellent fit in all but one case, that for a/d of 2.0.

5.) Lift forces alternate due to the nature of vortex generation and shedding but are not necessarily symmetric about zero force. This would make twice the peak force greater than twice the semi peak to peak or average.

APPENDIX

INSTRUMENT LIST

INSTRUMENT		MANUFACTURER/MODEL
BRIDGE AMPLIFIER	———	VISHAY/BAM-1
FILTER POWER SUPPLY	———	HEWLETT PACKARD/6205B DUAL CHANNEL
RECORDER	———	CLEVITE BRUSH/220
PROXIMITOR SYSTEM	———	BENTLY NEVADA/3115N 2388
OSCILLOSCOPE	———	TEKTRONIX/561 W3A6
SHAKER	———	LING/101
SHAKER POWER AMP	———	LING/POA-1
OSCILLATOR	———	HEWLETT PACKARD/202CD
FREQUENCY COUNTER	———	SIMPSON/2725A

REFERENCES

1. Sarpkaya, T., "Vortex Shedding and Resistance in Harmonic Flow about Smooth and Rough Circular Cylinders at High Reynolds Numbers," National Science Foundation Report NPS59SL 76021 Washington, D.C., February 1976.

2. Hunt, J. P., "The Fluid Resistance of Shrouded and Unshrouded Circular Cylinders in an Oscillatory Flow," Masters Thesis, University of Houston, Department of Mechanical Engineering, December 1973.

3. Heinzer, A. H., "Experimental Investigation of the Wake of an Oscillating Cylinder," Masters Thesis, University of Houston, Department of Mechanical Engineering, January 1968.

4. Isaacson, M. and Maull, D. J., "Transverse Forces on Vertical Cylinders in Waves," Trans. ASCE, J. Waterways and Harbors, 102 WW1 (1976), 49.

5. Schlichting, H. Boundary Layer Theory, McGraw Hill, 1968, pp. 24-42, 202-206.

6. Benedict, R. P., "Engineering Analysis of Experimental Data," Trans. ASME, J. Engr. Power, 91A, (1969), 21.

7. Chakrabarti, S., Discussion of reference 4, Trans. ASCE, J. Waterways and Harbors, 102WW4 (1976), 491.

8. Hamaan, F. H., "The Forces on Cylinders Oscillating Sinusoidally in Water," Masters Thesis, University of Houston, Department of Mechanical Engineering, August 1970.

9. Wiegel, R. L., and Delmark, R. C., "Wave Induced Eddies and 'Lift' Forces on Circular Cylinders," Ninth Symposium on Naval Hydrodynamics, Office of Naval Research, 1973.

10. Kline, S. J. and McClintoch, F. A., "Describing Uncertainties in Single Sample Experiments," Mechanical Engineering, 75 (1953), 3.